Rijksuniversiteit Groningen

Bachelor Thesis

Morphological asymmetry in mock HI observations of Simba galaxies

Author:
R.N. Talens
S4749898

Supervisors:
prof. dr. M.A.W. Verheijen
prof. dr. F. Fraternali
N. Hank

Abstract

The HI discs of galaxies are particularly sensitive to disruption from external influences, due to their extent to large radii. Asymmetries in a galaxy's HI morphology are therefore thought to leave clues of a galaxy's dynamical history, from which we could infer how it has interacted with its local environment. Since such interactions are often also responsible for the accretion or removal of gas, which play a crucial role in galaxy evolution, characterizing how these external processes induce asymmetries in HI morphology could reveal the importance of such processes and local environment in the evolution of galaxies. In this study, we set out to examine the changes in morphological HI asymmetries for a sample of 36 simulated galaxies that had experienced mergers, tidal interactions, or were isolated. The galaxies were simulated with the SIMBA simulations, from which we produced mock HI cubes with properties similar to real observations. We have quantified the HI asymmetry using the A_{mod} parameter, which makes use of the moment-0 map, and investigated trends in asymmetry over 11 snapshots in time, spanning a total of $\sim$2.3 Gyr. The majority ($\sim$67%) of our isolated galaxies were either stable in their asymmetry or slightly decreasing. Furthermore, we found that for all galaxies in our sample that experienced tidal interactions with a companion galaxy, the interaction induced significant increases ($>$10%) in the mean asymmetry within the time frame of the interaction. Finally, we also found that while our sample of merging galaxies tended to increase in HI asymmetry as a result of the interaction during the merging process, their asymmetry followed a decreasing trend after their highest increase in baryonic mass in most cases ($\sim$64%). The steepness of this trend could possibly be inversely related to the duration of the merging process. These findings imply a strong correlation between the various environmental influences a galaxy is subject to and the asymmetry in HI morphology of the galaxy. These results also further highlight the importance environment likely has on galaxy evolution, due to the connection between the examined mechanisms and gas removal and accretion.

Contents

1 Introduction **4**

2 Methods **7**
2.1 Asymmetry index 7
2.2 The SIMBA simulations 8
2.3 HI mock data 9
2.3.1 Our galaxy sample 9
2.3.2 MARTINI cube extraction 10
2.3.3 Masking the HI cubes 10
2.3.4 Smoothing of the moment-0 maps 11
2.4 Determining the kinematic and HI morphological center 11

3 Results **16**
3.1 Isolated galaxies 16
3.2 Interacting galaxies 18
3.3 Mergers 22
3.4 Comparison of the centers 24

4 Discussion **27**
4.1 Peculiarities in the categories 27
4.1.1 Isolated galaxies 27
4.1.2 Mergers 27
4.2 Limitations 30

5 Summary and Conclusions **31**

1 Introduction

One of the earliest attempts of galaxy classification based on appearance was famously done by Hubble (1926), and ever since it has been evident that galaxies can vary greatly in their overall morphology. Prominent differences can be seen in their global appearance, such as a spiral, elliptical, or irregular shape, including the presence of bars or winding patterns of the spiral arms. The morphology of a galaxy is determined by its evolution, which is driven by both internal processes and external processes. Due to their stochastic nature, external processes can produce asymmetries in the distribution of the baryonic mass, and analyzing those can enable us to reconstruct the processes that might have taken place (Sancisi et al., 2008).

In general, external processes are likely to leave prominent marks on the neutral atomic hydrogen (HI) discs due to their extent to very large radii, where the gravitational potential is very shallow. Indeed, there have been numerous observations of asymmetries in HI morphology. Most notably, Hibbard et al. (2001) made a compilation of HI maps of optically peculiar galaxies observed by various contributors, and present 181 objects with asymmetric HI discs. Common examples of asymmetric features in HI morphology are tidal tails (Duc and Bournaud, 2008) or "lopsidedness", a term coined by Baldwin et al. (1980) to refer to galaxies with largely offset HI discs relative to their stellar disc.

Various external mechanisms are proposed to induce asymmetries in a galaxy's HI distribution. For example, galaxies in high density environments can experience ram pressure stripping: a process first suggested by Gunn and Gott (1972) that describes how gas is stripped from the galaxy due to the pressure from moving through the hot intracluster medium. This is seen in action in D100 for instance, a spiral galaxy in the Coma cluster with an impressively long tail due to ram pressure stripping (Cramer et al., 2019). Other examples of external processes that are suggested to affect galaxy HI morphology are tidal interactions with other galaxies (Mapelli et al., 2008), mergers (Zaritsky and Rix, 1997), or gas accretion from cosmic filaments (Bournaud et al., 2005). Figure 1 shows how the HI distribution of three galaxies in the M81 Group is disturbed due to a three-way tidal interaction between Messier 81, Messier 82 and NGC 3077, creating bridges of HI between the galaxies (Chynoweth et al., 2008). It is clear from this image that there exists a possible correlation between the HI morphology of a galaxy and its environment. Indeed, Deb et al. (2023) conducted a study on the effects of environment for galaxies in the Abell 2626 cluster, and found that isolated galaxies are less likely to be asymmetric compared to galaxies in the substructures of the cluster, attributing this to tidal interactions likely being more efficient within these substructures. Reynolds et al. (2020) studied the impact of the local environment on different types of HI asymmetries for ∼140 objects, and found a possible trend between morphological asymmetry and the local environment density. The strongest trend with environment density was found for the spectral asymmetry, and the spectral and morphological asymmetries were also found to be moderately correlated.

Until recently, spatially resolved HI observations have only been available for a few hundred galaxies nearby, which has led there to be comparatively few studies that quantify morphological HI asymmetry. Nonetheless, several techniques have been developed in attempts to quantify these morphological asymmetries. For instance, Lelli et al. (2014) developed an asymmetry parameter that reliably quantified asymmetries in the outskirts of HI discs. Another quantitative method of determining morphological asymmetry is through the use of Fourier analysis as used by Angiras et al. (2006), who used the normalized amplitude of the m = 1 Fourier component to compare morphological HI asymmetries for galaxies in the Eridanus group. Fortunately, the newest untargeted HI surveys from the Square Kilometre Array (SKA) and its pathfinders telescopes are promising in terms of providing more spatially resolved HI maps, which will allow

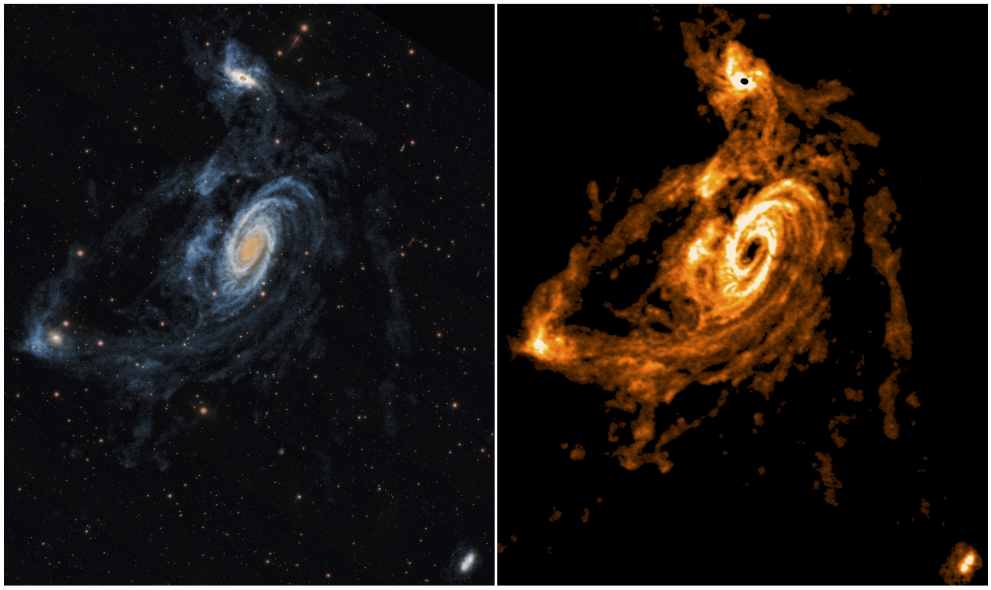

Figure 1: The HI distribution of the interacting triplet Messier 81, Messier 82 and NGC 3077. The right image shows the HI distribution, and the left image shows this data superimposed on a color image of the Sloan Digital Sky Survey. Image taken from de Blok et al. (2018).

for more detailed investigations on HI morphology. Shallow surveys such as the Shallow Northern-sky Survey (SNS, Adams and van Leeuwen 2019) with the APERture Tile In Focus (Apertif, Verheijen et al. 2008; van Cappellen et al. 2022) system on the Westerbork Synthesis Radio Telescope (WSRT) and the Widefield ASKAP L-band Legacy All-sky Blind Survey (WALLABY, Koribalski et al. 2020) from the Australian SKA Pathfinder (ASKAP, Johnston et al. 2008; Hotan et al. 2021) will provide thousands of spatially resolved HI maps for nearby galaxies. Local volumes are observed by the MeerKAT International GHz Tiered Extragalactic Exploration (MIGHTEE-HI, Jarvis et al. 2016; Maddox et al. 2021 survey and the Medium-Deep HI imaging survey (MDS, Verheijen et al. 2009) with Apertif. Together, these surveys will provide many spatially resolved HI maps at low redshifts, which will enable extensive and detailed statistical studies on asymmetry in HI morphology.

Thanks to advancements in numerical modeling, cosmological hydrodynamical simulations are able to produce a realistic galaxy population that can be used to study HI asymmetries. Simulated galaxies can be "observed" like a real population, and simulations can then aid in interpreting observational data or understanding the physical origin of the asymmetries. Manuwal et al. (2021) utilized the EAGLE simulations (Schaye et al., 2014) to examine drivers of HI asymmetry, and found that satellite galaxies are more asymmetric on average than central galaxies, attributing this to ram pressure and tidal stripping. This is further supported by Watts et al. (2020), who also examined the conditions under which HI asymmetries may arise. Using the IllustrisTNG simulations (Nelson et al., 2017) and taking halo mass as a proxy for environment, they also observed that satellite galaxies are more asymmetric as a population than central galaxies. While these studies mainly investigated asymmetries in the HI line profiles, Reynolds et al. (2020) showed that this may be correlated to asymmetries in HI morphology. However, we are not aware of extensive use of simulations in literature to study such asymmetries directly. Nonetheless, the studies mentioned above serve to illustrate the usefulness of hydrodynamical simulations for research related to the HI content of galaxies, and the prospect of utilizing them to help our understanding of morphological HI asymmetries in real galaxies seems promising.

Some of the environmental processes mentioned earlier are often responsible for gas accretion into (e.g. mergers) or gas removal (e.g. tidal interactions, ram pressure stripping) from galaxies, and so are likely crucial for galaxy evolution (i.e. enhancing or inhibiting star formation). Because of the sensitivity of the outer regions of the HI discs to these external influences, morphological asymmetries in HI distributions are likely to be good indicators of such mechanisms and so allow us to make inferences about a galaxy's dynamical history. Simulations further provide a unique advantage in their ability to give direct insight on a galaxy's state at different points in time, and so could be used to uncover how a galaxy's dynamical history has contributed to changes in its HI morphology over time. While morphology alone cannot tell us the exact processes going on within a galaxy, it could still highlight the different influences of a galaxy's local environment on its evolution. Furthermore, the sheer amount of HI data that will be provided by the newest generation of HI surveys could allow us to reconstruct the evolution of these environmental processes by studying asymmetries at different stages of mergers and interactions.

That is in essence the goal of this study. We wish to characterize the effects on the HI morphology of galaxies of a variety of environmental processes, hoping to be able to use asymmetry measurements in real data in the future to understand the processes that have caused and how these processes contributed in their evolution. We do this by analyzing the evolution of the morphological HI asymmetry for a sample of 36 simulated galaxies, assigned into three categories: isolated, interacting, and merging galaxies. The categories were chosen to roughly represent some of the interactions a galaxy might have with its environment in reality. The sample of galaxies is extracted from the SIMBA simulations (Davé et al., 2019), from which we produce synthetic mock HI data cubes with MARTINI (Oman, 2019) that are designed to match observations of a population in the Abell 262 galaxy cluster from the MDS. This sample is part of a larger selection of simulated galaxies of which the different types of asymmetries will be studied in more detail and compared to real MDS data of the Abell 262 cluster. With the robust A_{mod} parameter developed by Lelli et al. (2014), we quantify the asymmetry of our galaxies across 11 snapshots over a time frame of $\sim$2.3 Gyr. From there, we examine the changes in asymmetry of the HI discs of our galaxies for each of our categories, possibly highlighting unique trends among the different mechanisms they represent.

The thesis is structured as follows. Our methodology is laid out in Chapter 2. More specifically, Section 2.1 describes how we quantify asymmetry with the A_{mod} parameter. Section 2.2 describes the SIMBA simulations (Davé et al., 2019). Section 2.3.1 provides a more detailed description of our galaxy sample and the categories (merger, interaction, isolated), and Section 2.3.2 describes how we produce mock HI data from the simulations with the MARTINI software (Oman, 2019). We present and analyze our main results in Chapter 3, discussing our three categories first and then investigating an appropriate center of rotation for observations in Section 3.4. Chapter 4 contains a discussion on some individual galaxies and the limitations of this work. Finally, a summary of our key results, our conclusions and their implications are laid out in Chapter 5.

2 Methods

The following chapter details the methodology used in this work. Firstly, Section 2.1 describes the parameter used to quantify the morphological asymmetry. Section 2.2 then provides a description of the SIMBA simulations, which were used to simulate our galaxies and their environments. Our galaxy sample and the production/processing of synthetic HI cubes from the simulations are described in Section 2.3. Finally, Section 2.4 explains how the HI morphological and kinematic centers were obtained.

2.1 Asymmetry index

Introduced by Schade et al. (1995), the asymmetry index is a way of quantifying a galaxy's asymmetry. It is defined as:

$$A = \frac{\sum_{i,j} |I(i,j) - I_{180}(i,j)|}{2\sum_{i,j} |I(i,j)|}, \tag{1}$$

where $I(i,j)$ denotes the intensity at position (i,j) in the original image of the galaxy on the sky plane and $I_{180}(i,j)$ denotes the the intensity at the same position (i,j) in the image rotated 180° around a specified point. Thus, one calculates the sum of the difference between the pixels of the original and rotated image, and normalizes this residual by the total intensity of the image. The asymmetry can have values between 0 and 1: 0 being perfectly symmetric and 1 being highly asymmetric.

Since Equation (1) is weighted by the total intensity of the image, it will be dominated by the brightest pixels in the center of the galaxy. We are interested in the asymmetry of the HI disc of galaxies, and it is often the fragile outer parts of this disc that are most disturbed by external influences like tidal interactions and ram pressure stripping. For this purpose, Lelli et al. (2014) introduced the so-called modified asymmetry index (denoted as $A_{\rm mod}$ from here), defined as:

$$A_{\rm mod} = \frac{1}{N}\sum_{i,j}^{N} \frac{|I(i,j) - I_{180}(i,j)|}{|I(i,j) + I_{180}(i,j)|}, \tag{2}$$

where N denotes the total number of nonzero pixels in either the added or subtracted images. In this equation, the residual is instead normalized by the local flux density of the image, and so is more sensitive to asymmetries in the low density regions typical of the outer HI disc.

$A_{\rm mod}$ depends on several observational parameters, such as the HI column density threshold, resolution and signal-to-noise, as investigated by Bilimogga et al. (2022). Using the EAGLE simulations (Schaye et al., 2014), they compared $A_{\rm mod}$ values for various column density thresholds of 2, 5, 15, and $45 \times 10^{19}\,{\rm cm}^{-2}$ to $A_{\rm mod}$ for a reference threshold of $1 \times 10^{19}\,{\rm cm}^{-2}$. They found that irrespective of resolution, the column density threshold of $5 \times 10^{19}\,{\rm cm}^{-2}$ provided $A_{\rm mod}$ values within 10% of those at the reference threshold for almost all galaxies in their sample. They therefore recommend adopting an upper limit of $5 \times 10^{19}\,{\rm cm}^{-2}$ for the column density threshold when investigating processes affecting the outer regions of HI discs.

In this study, we quantify the asymmetry in the HI discs of our simulated galaxies with the $A_{\rm mod}$ parameter, as described by Equation (2). The calculation will be done on the moment-0 maps (a map of integrated spectral line intensity) obtained from the mock HI cubes (see Section 2.3.2) of our galaxies. The minimum of the galaxy's gravitational potential will be taken as the center of rotation throughout most of this study, but we also examine if the kinematic center and morphological center yield similar results (see Section 3.4). We adopt an HI column density threshold of $5 \times 10^{19}\,{\rm cm}^{-2}$, as proposed by Bilimogga et al. (2022), and remove any pixels with values below this from the moment-0 maps.

2.2 The SIMBA simulations

The SIMBA simulations (Davé et al., 2019) is a suite of cosmological galaxy formation simulations based on GIZMO, a meshless finite mass hydrodynamics + gravity solver that marries smooth particle- and mesh-based approaches (Hopkins, 2015). It is a descendant of the MUFASA simulations (Davé et al., 2016), and aims to improve and build on much of its functionality. It assumes a Λ-cold dark matter cosmology with parameters $\Omega_m = 0.3, \Omega_\Lambda = 0.7, \Omega_b = 0.048, H_0 = 68\,\mathrm{km\,s^{-1}\,Mpc^{-1}}, \sigma_8 = 0.82$, and $\mathrm{n}_s = 0.97$ from the Planck Collaboration XIII (2016).

Radiative cooling and photo-ionization heating are handled using the GRACKLE-3.1 library (Smith et al., 2017), including non-equilibrium evolution of primordial elements and metal cooling. The adiabatic and radiative terms are evolved together in the cooling sub-time-step, resulting in a more accurate thermal evolution compared to MUFASA's approach of evolving the system adiabatically over the full time-step and applying cooling after. Self-shielding is also included self-consistently with an ionizing background that is attenuated depending on the gas density, based on the prescription provided by Rahmati et al. (2013).

SIMBA further improves on its parent MUFASA in how it models black hole growth and active galactic nucleus (AGN) feedback. Where MUFASA did not explicitly model black hole accretion and its interaction with the surrounding gas, SIMBA handles black hole growth with a torque-limited accretion model from Anglés-Alcázar et al. (2017) when accreting from cold ($\mathrm{T} < 10^5\,\mathrm{K}$) or star-forming gas. In this model, the gas inflow rate is driven by disc gravitational instabilities as described by Hopkins and Quataert (2011). SIMBA applies Bondi accretion when accreting from hot gas ($\mathrm{T} > 10^5\,\mathrm{K}$), as it is a more physically appropriate model in that case (Bondi, 1952).

The simulations incorporate three different kinds of AGN feedback to quench galaxies with: radiative mode AGN winds, AGN jets, and X-ray feedback. The chemical enrichment model tracks the enrichment of 11 metals, with enrichment from Type II supernovae, Type Ia supernovae and Asymptotic Giant Branch stars. Galactic winds driven by star formation are modeled similarly as in MUFASA, which uses decoupled two-phase winds heated by Type 1a supernovae and AGB stars, but with an updated model to give more accurate mass outflow rates.

Star formation is modeled with an $\mathrm{H_2}$ star formation law based on the model used in MUFASA. Here, the star formation rate is determined by the $\mathrm{H_2}$ fraction and dynamical time (t_{dyn}) as described by a Schmidt (1959) law:

$$\mathrm{SFR} = \frac{\epsilon_* \rho f_{\mathrm{H2}}}{t_{\mathrm{dyn}}}, \tag{3}$$

where the efficiency of star formation is taken to be $\epsilon_* = 0.02$ (Kennicutt, 1998). The $\mathrm{H_2}$ mass fraction is determined by:

$$f_{\mathrm{H2}} = 1 - 0.75\frac{s}{1 + 0.25s}, \tag{4}$$

where

$$s = \frac{\ln\left(1 + 0.6\chi + 0.01\chi^2\right)}{0.0396\, Z(\Sigma/\mathrm{M_\odot pc^{-2}})}, \tag{5}$$

where Z is the metallicity in solar metallicity, Σ is the local column density, and χ is a function of metallicity (Krumholz et al., 2009). A minimum number density of $\mathrm{n_H} > 0.13\,\mathrm{cm^{-3}}$ is required for a gas element to be considered as part of the interstellar medium and to be able to spawn a star particle. A star particle is created stochastically from a single gas element, and will have equal mass and metallicity as its parent.

A fast approximate friends-of-friends (FOF) finder is applied to star particles, dense gas elements and black holes to group them into galaxies during the simulation run. It does this by

identifying neighbours within a cube of $2\mathcal{L}$, where $\mathcal{L}$ is the linking length (a threshold distance under which particles are considered to be linked). This approach allows the FOF finder to run at every time step due to its computational speed. Various galaxy and halo properties are then calculated throughout the simulation run, and are stored in standalone HDF5 catalogues for each snapshot with CAESAR: a Python package based on the **yt** visualization and analysis toolkit (Turk et al., 2010). These catalogues provide extensive information on the simulated galaxies and haloes, such as particle lists, group ID's and a variety of physical properties.

SIMBA has several runs to choose from, simulating a co-moving volume of various sizes and mass resolutions. In this study, we used their flagship $100\,\mathrm{Mpc}\,h^{-1}$ run, which evolves a $(100\,\mathrm{Mpc}\,h^{-1})^3$ volume initialized with 1024^3 gas elements and 1024^3 dark matter particles. This corresponds to a mass resolution of $1.82\times10^7\,\mathrm{M}_\odot$ and $9.6\times10^7\,\mathrm{M}_\odot$ for gas elements and dark matter particles respectively. We supplement our sample with galaxies from their $25\,\mathrm{Mpc}\,h^{-1}$ run, which instead evolves a $(25\,\mathrm{Mpc}\,h^{-1})^3$ box initialized with 2×512^3 particles. This run corresponds to a mass resolution of $2.28\times10^6\,\mathrm{M}_\odot$ and $1.2\times10^7\,\mathrm{M}_\odot$ for gas elements and dark matter particles respectively. The input physics for both runs are identical.

2.3 HI mock data

2.3.1 Our galaxy sample

Our sample of galaxies was selected from a larger sample of galaxies that was constructed to match MDS observations, on which the final asymmetries will be studied in more detail (private communications, N. Hank and M.A.W. Verheijen). The galaxies in this sample are placed at a distance of 71.86 Mpc, which is the median distance to the Abell 262 galaxy cluster (Choque-Challapa et al., 2021). This distance was chosen to simulate a population of galaxies similar to that in the cluster from the MDS, and the galaxies have randomly assigned inclinations and viewing angles.

The parent sample assigned the galaxies into the following categories: mergers, interacting and isolated. The mergers are defined as galaxies that experience an increase of >5% in both their stellar and baryonic mass within the considered time frame. Galaxies in the interacting category are defined to have had a companion galaxy with >5% of the target galaxy's baryonic mass within 100 kpc of our target galaxy for at least one snapshot in the considered time interval, without the aforementioned increase in mass (which would classify them as mergers). Isolated galaxies were then defined to be galaxies that fit into neither of these categories, meaning that there was no companion galaxy within 100 kpc of the target galaxy with >5% of the target's baryonic mass. We note that this means there could still be a companion galaxy within 100 kpc that does not fulfill the >5% criterion, or that there is a more massive galaxy outside of this 100 kpc box. Indeed, we found one galaxy isolated where the former seemed to be the case (see Section 3.1). From each of these three categories, we selected 12 galaxies, resulting in a sample of 36 galaxies in total.

The galaxies in the parent sample were grouped into mass bins with ranges $9.79 \leq \log \mathrm{M_{bar}} < 10.08$, $10.08 \leq \log \mathrm{M_{bar}} < 10.35$, $10.35 \leq \log \mathrm{M_{bar}} < 10.63$, and $10.63 \leq \log \mathrm{M_{bar}} < 11.5$. Our sample consists of galaxies with varying A_{mod} values at the last snapshot. Out of each of these four mass bins, we picked three galaxies for our selection: one with low ($A_{\mathrm{mod}} < 0.3$), one with medium ($0.3 < A_{\mathrm{mod}} < 0.6$) and one with high ($A_{\mathrm{mod}} > 0.6$) asymmetry, resulting in a total of 12 galaxies per category. This A_{mod} was calculated at a resolution of ∼10 beams within the $5\times10^{19}\,\mathrm{cm}^{-2}$ contour. The motivation behind this resolution specifically is explained in Section 2.3.4.

2.3.2 MARTINI cube extraction

To produce mock data cubes from the SIMBA simulations, we used MARTINI: an object-oriented Python package developed to extract synthetic HI data cubes from smooth particle hydrodynamical simulations (Oman, 2019, 2024). A more detailed explanation of how MARTINI produces the mock cubes can be found in Oman et al. (2018), but will be briefly summarized here.

MARTINI calculates the HI gas fraction within each gas element of the central galaxy, following the same prescription for self-shielding and background radiation as is used in SIMBA, from Rahmati et al. (2013). A coordinate system is adopted that sets the minimum gravitational potential of the galaxy as the center. The coordinate system aligns the x-axis with the specific angular momentum vector of the HI disc.

MARTINI takes a fixed aperture of 100 kpc to extract the target galaxy and its surroundings from the simulations. The pixels in the final mock data cubes have units of Jy beam^{-1}, which we convert to units of cm^{-2}. The equation used for the conversion is:

$$\left(\frac{N_{\rm HI}}{\rm cm^{-2}}\right) = 1.10 \times 10^{24}(1+z)^2 \times \left(\frac{S^{V_{\rm obs}}}{\rm Jy\ km\ s^{-1}}\right)\left(\frac{ab}{\rm arcsec^2}\right)^{-1}, \tag{6}$$

where z is the redshift to the galaxy (set to $z = 0.0163$, the redshift of the Abell 262 cluster), a and b are the semi-minor and semi-major axes of the beam, and $S^{V_{\rm obs}}$ is the integrated flux in the observed velocity frame (Meyer et al., 2017). Each mock cube has a surface of 175 × 175 pixels with pixel size 5" × 5", and 128 velocity channels with a channel width of 7.86 km s^{-1}. All the cubes are then convolved with a 15" circular Gaussian beam, leading to a resolution that corresponds ∼1.74 kpc per pixel at the chosen distance of 71.86 Mpc. A cube was extracted at 11 snapshots (snapshot number 140 through 150) in time for each galaxy, corresponding to a redshift range of $0 < z < 0.2$ or ∼2.3 Gyr, with a spacing varying from $z \simeq 0.0169$ to $z \simeq 0.0189$. For the purpose of this study, no noise was added to the cubes. In real data, this would correspond to a high signal-to-noise. We generate the moment-0 maps from the cubes by integrating over the spectral (velocity) axis.

2.3.3 Masking the HI cubes

Due to MARTINI's fixed aperture, any HI emission of a companion galaxy located within the 100 kpc box of the target galaxy will be included in the data cube. This HI emission will contribute to the calculated asymmetry if left in the moment-0 map. Since we wish to only examine the evolution of the asymmetry of our target galaxies, we apply a mask that isolates the target galaxy from this companion HI emission.

The removal of unwanted HI emission from the companion was done with a script using the OBJECTS task in GIPSY (Vogelaar and Terlouw, 2001). The script separates the largest object closest to the center. It does this by identifying all independent 3D objects using a column density threshold of 1×10^{19} cm^{-2} over 25 km s^{-1} that consist of at least five velocity channels. From there, a 3D mask of the most massive object closest to the center is constructed. This mask is then applied to the data cube, leaving the companion out so that only our target galaxy resides in the cube. Due to the use of this column density threshold as an indication of the independence of objects, we sometimes found that two galaxies that are particularly connected were not properly separated, meaning that the companion was still included in the asymmetry calculation. However, higher density thresholds were either still unsuccessful or removed excessive low density HI from our target galaxy. Fortunately, this was only the case for the merging galaxies and two of our interacting galaxies. For the mergers, we thought it was fitting to consider them

as one system regardless, and the two interacting systems were taken into consideration in further analysis.

2.3.4 Smoothing of the moment-0 maps

Since the asymmetry parameter is calculated pixel-wise, its value is dependent on the resolution of the image. As explained in Section 2.1, Bilimogga et al. (2022) found that the asymmetry parameter of a galaxy is reduced as the galaxy is resolved by less beams. For this study, we wish to have the galaxy be resolved by ∼10 beams across the surface enclosed by a contour of $5 \times 10^{19}\,\mathrm{cm}^{-2}$, which is the threshold we use for our A_{mod} (see Section 2.1). While angular resolution is often quantified with the number of beams across the semi-major axis, we chose to quantify it with the number of beams across the surface within our threshold contour instead. This is motivated by the fact that a face-on galaxy is likely to have more beams across its surface than an edge-on galaxy with the same semi-major axis, and will therefore also have more pixels contributing to its A_{mod}. Although ∼10 beams across the surface leads to a relatively low spatial resolution and loss of detail in a galaxy's HI morphology, many of the HI maps from the untargeted HI surveys from the SKA pathfinders will have similar resolutions.

To accomplish this spatial resolution of ∼10 beams across the surface, we smoothed our moment-0 maps to five extra resolutions (in addition to the native 15" resolution), corresponding to beam sizes of 30", 45", 60", 90" and 120". The chosen resolution was then determined by which moment-0 map came closest to having ∼10 beams within the aforementioned contour. Finally, we impose a criterion of a minimum of 5 beams and no more than 15 beams within a galaxy's contour, to limit variation in beam size across different galaxies.

The moment-0 maps showed that some galaxies in our sample change size considerably from one snapshot to the next. Figure 2 shows how the number of beams is distributed across all snapshots for every galaxy. Indeed, the plot on the left (representing the distribution of the number of beams when a galaxy's best beam of snapshot 150 was used across all its snapshots) shows that a lot of snapshots fall outside of our specified 5-15 range for the number of beams. To keep to our constraint of ∼10 beams within a galaxy's contour for all of our images, we opted for an adaptive approach to our resolution choice and instead evaluated the best fitting beam on a case-by-case basis for each individual snapshot. For this purpose, we identified the resolution that corresponded to ∼10 beams across the surface for each snapshot individually, and used this resolution to calculate A_{mod} for that snapshot. The distribution of the number of beams from this approach is shown in the plot on the right of Figure 2. We see much less spread in the number of beams, and all of them are within our required range of 5 to 15 beams within the contour. Figure 3 shows a mosaic of the original unmasked and unsmoothed moment-0 maps of a galaxy in the merger category, and Figure 4 shows the masked and smoothed moment-0 maps of the same galaxy, illustrating the effects of this approach.

2.4 Determining the kinematic and HI morphological center

Throughout this thesis, we take our center of rotation to be the center of the moment-0 map we are calculating A_{mod} from. As explained in Section 2.3.2, MARTINI adopts a coordinate system for the mock HI cubes that establishes the minimum of the galaxy's gravitational potential as the cube center. However, the location of the potential minimum is not something one has access to in real observations. There is also the possibility of galaxies dominated by stellar mass to have offset HI discs relative to the potential minimum. We therefore want to consider the HI morphological center and the kinematic center as proxies for the potential minimum which are two centers easily accessible in observations.

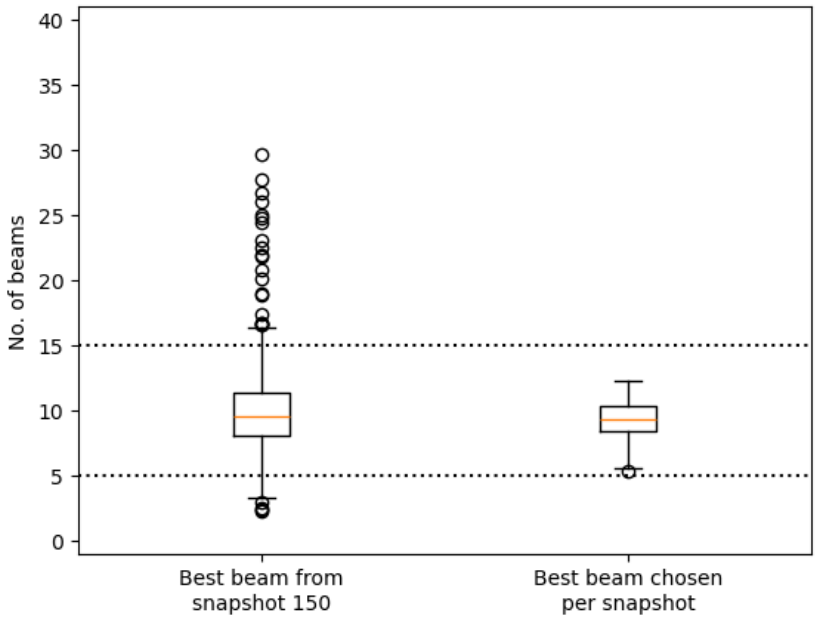

Figure 2: The distribution of the number of beams across all snapshots and galaxies for two different scenarios: choosing the resolution based on which fits best in the final snapshot (*left*), and choosing a beam on a case-by-case basis, evaluating what the best resolution is per snapshot (*right*). The orange line indicates the median number of beams, the boxes show the interquartile range (IQR), and the whiskers indicate the points of 1.5 × IQR. Points outside this 1.5 × IQR are considered "fliers" and are displayed individually. The area between the dotted lines represents the specified 5-15 range.

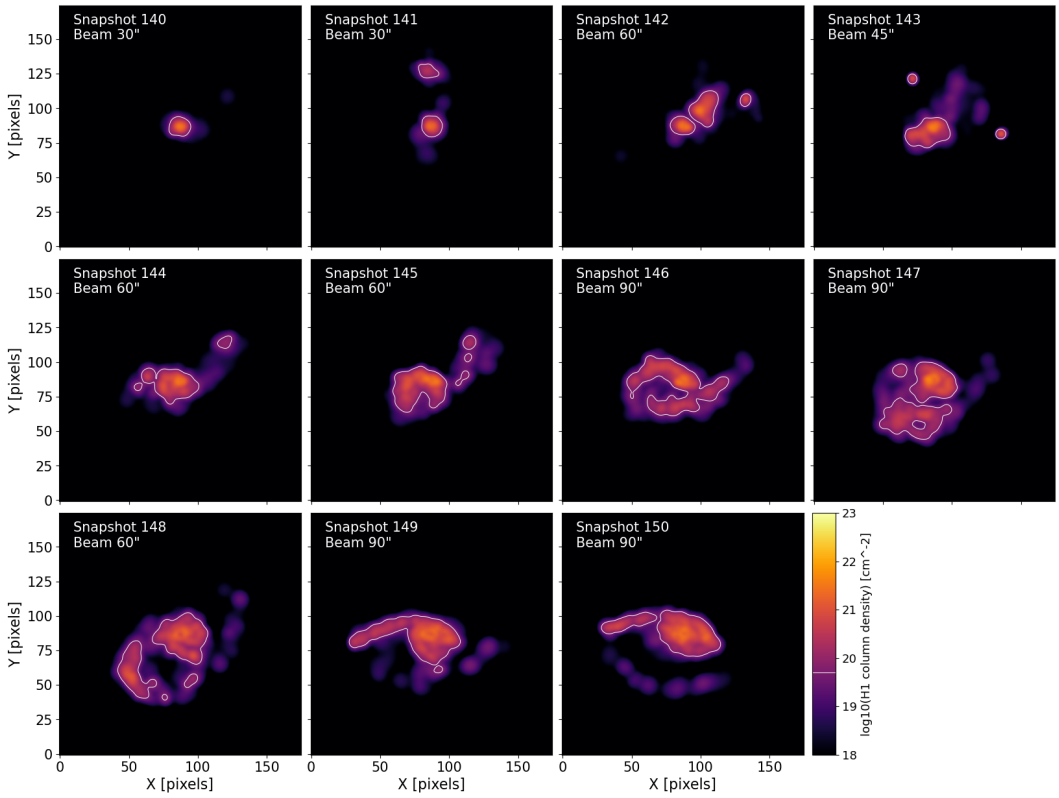

Figure 3: The unmasked and unsmoothed moment-0 maps of a galaxy in the merger category. The snapshot number is given in the top left of each map. The resolution of all moment-0 maps is 15". The white contour shows where the HI column density is $5 \times 10^{19}\,\mathrm{cm}^{-2}$.

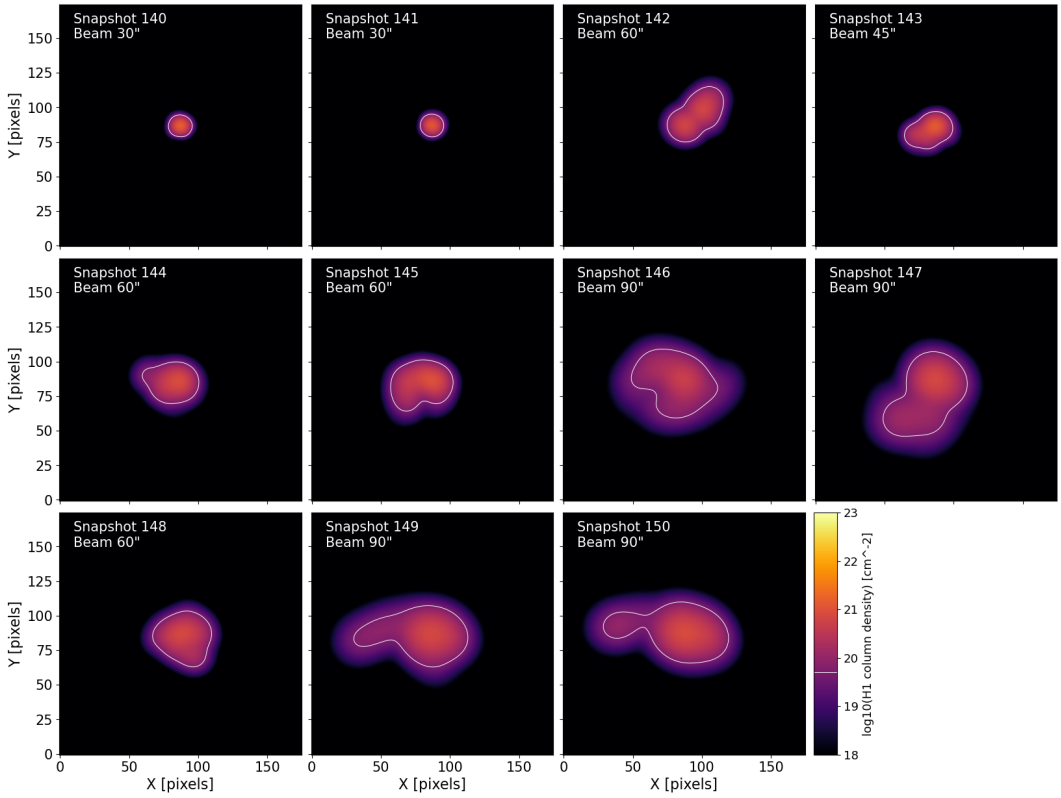

Figure 4: The masked and smoothed moment-0 maps of the galaxy in Figure 3. The snapshot number and resolution are given in the top left of each map. The white contour shows where the HI column density is $5 \times 10^{19}\,\mathrm{cm}^{-2}$.

The morphological center of our galaxies was calculated via a relatively simple 2D "center of mass" calculation. For this calculation, we calculated the intensity-weighted average of all the pixel coordinates, similar to how one would calculate the center of mass with the pixel intensities being analogous to their masses.

For the kinematic center, we created two additional moment maps of our galaxies: the moment-1 map (a map of the intensity-weighted velocity) and the moment-2 map (a map of velocity dispersion). The equations for the two moments are:

$$M_1 = \frac{\int v I_v dv}{\int I_v dv}, \tag{7}$$

$$M_2 = \frac{\int I_v (v - M_1)^2 dv}{\int I_v dv}, \tag{8}$$

for the moment-1 and moment-2 respectively, where I_v is the intensity and v the velocity.

In general, a galaxy with a regularly rotating disc in differential rotation will have a peak in its moment-2 map around the kinematic center, because the beam element there "captures" the receding and approaching parts simultaneously and so the velocity dispersion will be very high. We can then combine the two maps to estimate the kinematic center by looking for regions of high velocity dispersion along the contour of the galaxy's systemic velocity. Figure 5 shows an example of a moment-1 and moment-2 map side by side. The receding and approaching parts of the rotating disc are clearly visible in the moment-1 map, with the galaxy's systemic velocity in between (where there is no component of rotation along the line of sight). The moment-2 map shows a big peak in velocity dispersion along the systemic velocity contour. In our sample of galaxies, we looked for similar high dispersion regions near the systemic velocity contour, taken to be the mean value of all the nonzero pixels in the moment-1 map.

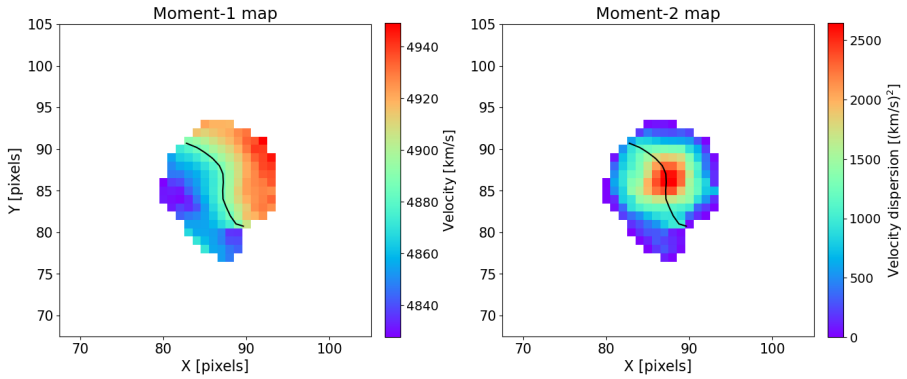

Figure 5: Examples of a moment-1 and moment-2 map of a galaxy, illustrating how the kinematic center was determined. The black contour in both maps represents the contour of systemic velocity.

3 Results

In this chapter, we present and analyze our results. Firstly, we want to take a moment to show a comparison of the variance in A_{mod} for our three categories in Figure 6. This figure would imply that the galaxies do not appear to be very different in how their asymmetries vary over time, irrespective of which category they were in. However, we stress that this figure on its own does not tell the whole story, and a more detailed investigation yields far more enlightening results in terms of trends in asymmetry. With that out of the way, the rest of this Section is structured as follows. Section 3.1, 3.2 and 3.3 discuss the results of our samples for the isolated, interacting and merger categories respectively. Section 3.4 discusses our findings regarding the HI morphological center and kinematic center as possible proxies for the potential minimum to be used in real observations.

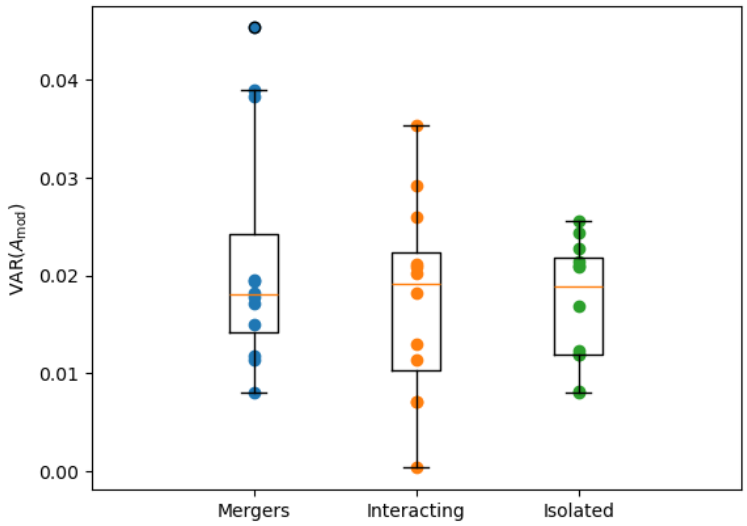

Figure 6: A comparison of how the A_{mod} variance for each galaxy in our three categories is distributed. The orange line indicates the median variance, the boxes show the interquartile range (IQR), and the whiskers indicate the points of 1.5 × IQR.

3.1 Isolated galaxies

The isolated sample consists of 12 galaxies that have had no companion with >5% of the target's baryonic mass within 100 kpc, nor the >5% stellar and baryonic mass increase that we consider to be the sign of a merger event. Figure 7 shows plots of A_{mod} across our considered snapshot range for our sample of isolated galaxies. Generally, one would expect isolated galaxies to stay relatively stable in their asymmetry over time compared to interacting or merging galaxies. However, it is still possible that a galaxy is recovering from an interaction or merger that happened prior to our considered time frame. This could then lead to some resulting asymmetries still being present for a few snapshots.

We categorize the isolated galaxy sample based on general trends in their A_{mod}, highlighting these general asymmetry trends with a Huber regression line: a robust line fitting method that is insensitive to outliers (Huber, 1964). Based on the slopes of their regression line, we categorized the isolated galaxies as increasing (slope $>$ 0.01), stable (-0.01 $<$ slope $<$ 0.01), or decreasing (slope $<$ -0.01) in A_{mod}. The resulting distribution is given in Figure 8. We see that 50% of

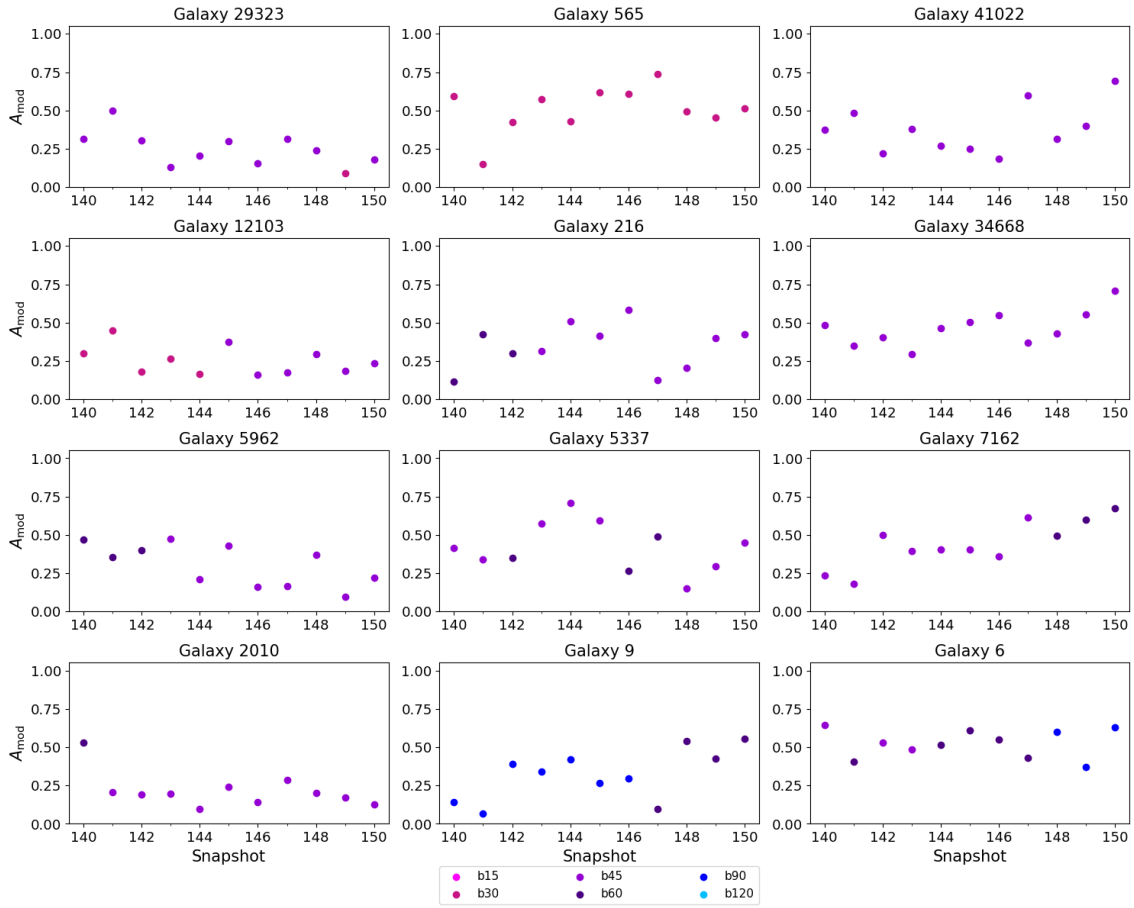

Figure 7: A mosaic of the evolution of A_{mod} across the considered snapshot range for our isolated galaxies. The meaning of the colors of the data points is displayed in the legend on the bottom, where b15 means a 15" beam, b30 means a 30" beam, etc. Galaxies in the same row are in the same mass bin.

our isolated sample displays stable behavior in $A_{\rm mod}$. Together with the ∼17% of galaxies with decreasing asymmetry, this accounts for ∼67% of our sample. ∼33% of the isolated galaxies show an increase in their asymmetries over time. The two galaxies with the steepest increases are further discussed in Section 4.1, along with a possible reason for the relatively high variance in this category. Still, these results suggest that isolated galaxies remain largely stable overall in their HI morphology. This is to be mostly expected, given that the morphology of isolated galaxies is often driven by their own gravitational potential and so is likely to be (and stay) symmetric.

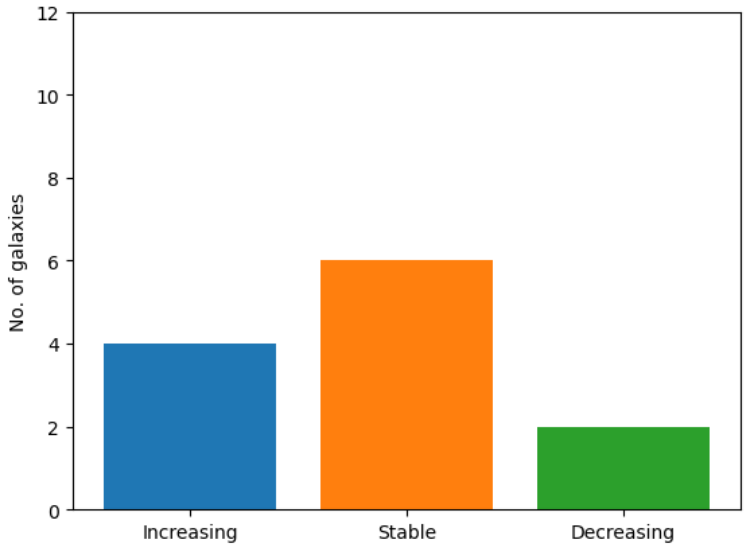

Figure 8: A distribution of how the $A_{\rm mod}$ of our isolated galaxies evolves. Galaxies are categorized as increasing, stable, or decreasing in $A_{\rm mod}$ over the entire considered time frame.

3.2 Interacting galaxies

Our interacting sample was defined to consist of galaxies that had a companion galaxy within the 100 kpc box surrounding our target with >5% of its baryonic mass, without leading to a >5% stellar and baryonic mass increase. Figure 9 shows $A_{\rm mod}$ plotted against the snapshot number for our 12 interacting galaxies. The difference in the spread of the red lines, which characterize the interactions as explained in the description of Figure 9, already suggests our sample experiences a variety of interactions, from very quick fly-by's, to more "involved" tidal interactions, and even a possible future merger. Figure 10 shows representative moment-0 maps for these different kinds of interactions. Note that these are the unmasked moment-0 maps with the companion included, and serve solely to illustrate the different nature of the interactions. No calculations were done on these maps.

Interacting galaxies are, by our own definition, isolated before the companion enters its 100 kpc box. This then allows us to investigate the effects an interaction has on the "original" asymmetry of our target galaxies. We categorized the interactions based on their percentage change in mean $A_{\rm mod}$ during the interaction relative to the mean $A_{\rm mod}$ before the interaction, denoted as $\Delta A_{\rm mod}$. The galaxies are then placed in the follow categories: increased ($\Delta A_{\rm mod} > 10\%$), unaffected ($-10\% < \Delta A_{\rm mod} < 10\%$), or decreased ($\Delta A_{\rm mod} < -10\%$). The time frame of the interaction is determined by the snapshots at which the companion has entered and left the 100 kpc box surrounding our target galaxy. Galaxy 359 and galaxy 782 were excluded from this

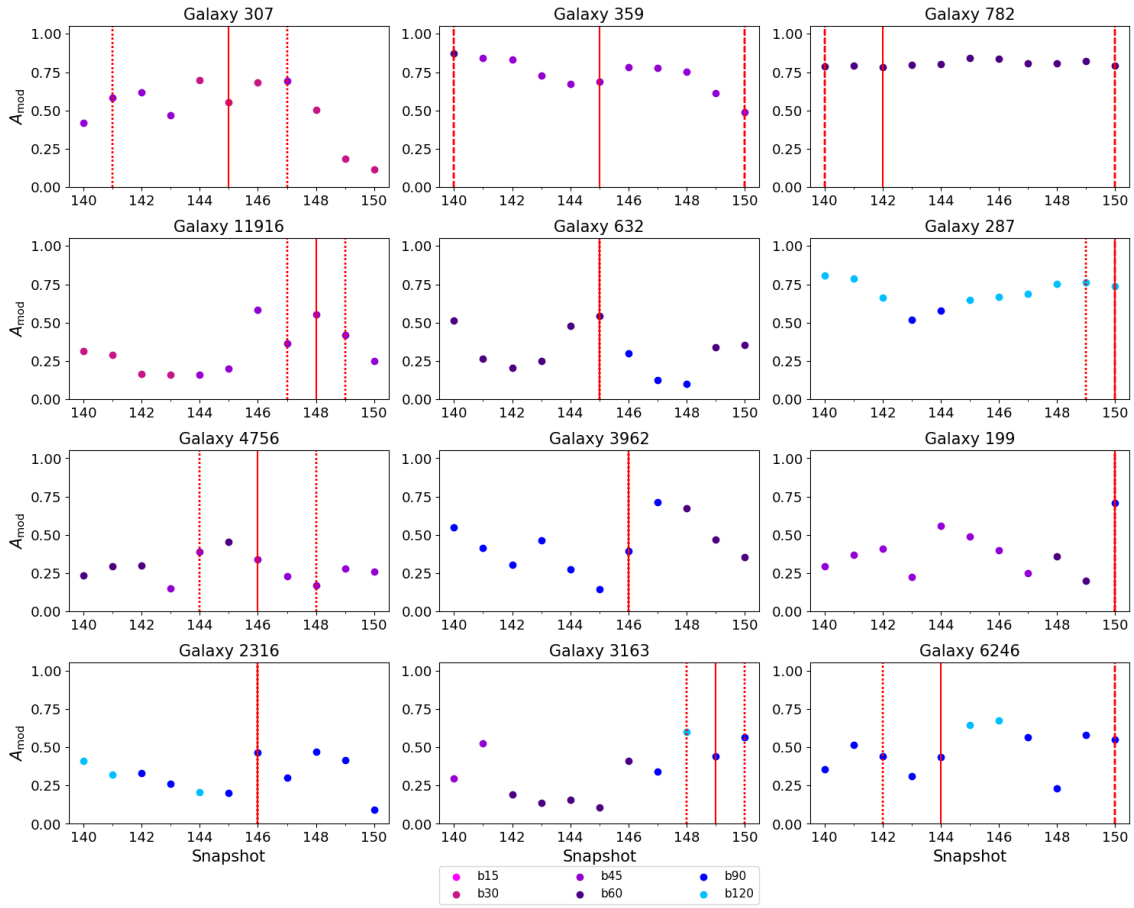

Figure 9: A mosaic of the evolution of A_{mod} across the considered snapshot range for our interacting galaxies. The dotted red lines indicate where the companion galaxy enters and leaves the 100 kpc box surrounding our target galaxy, while the dashed lines are used to indicate if the companion entered or left the box outside of our time frame. The solid red line indicates the pericenter (point of closest approach).

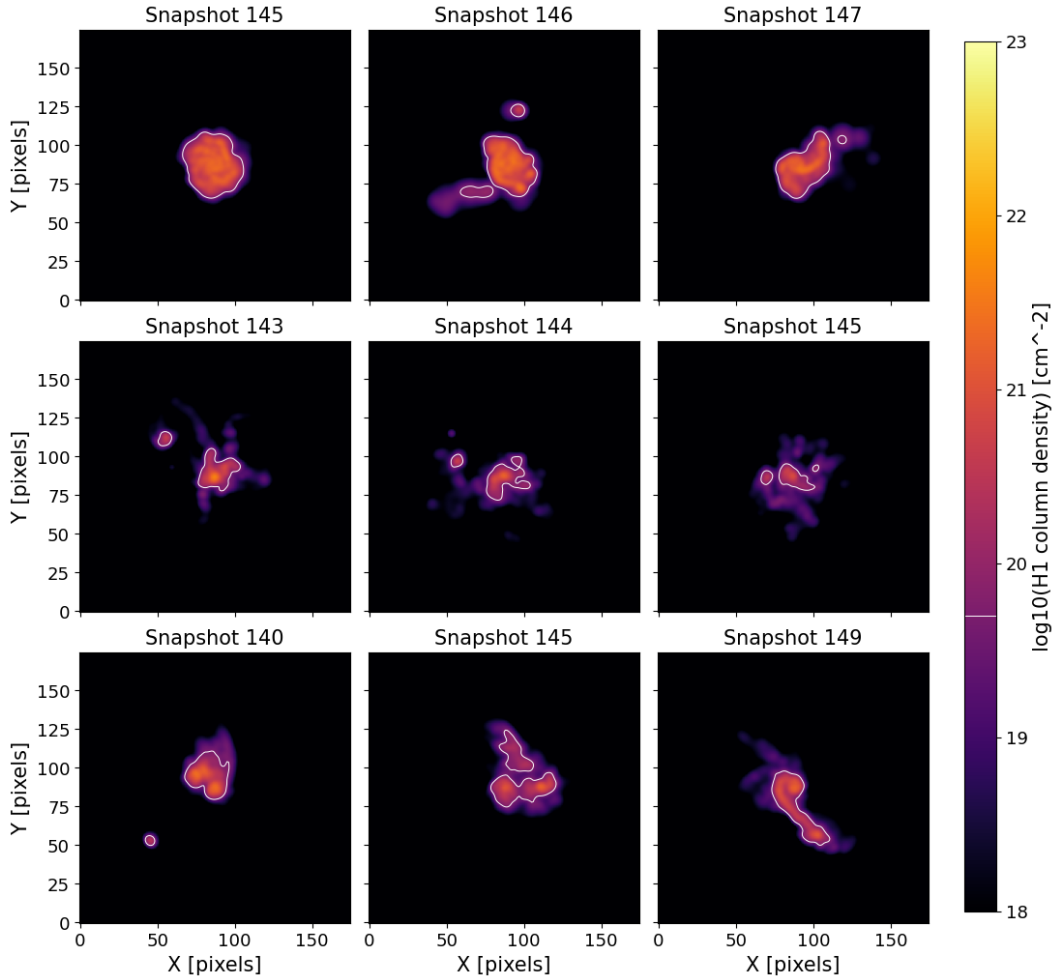

Figure 10: Some unmasked moment-0 maps representing the different kinds of interactions in our interacting sample: a quick fly-by with galaxy 3962 (*top*), a fairly close interaction with galaxy 307(*middle*), and a prolonged interaction suspected to result in a future merger 782 (*bottom*). The white contour shows where the HI column density is $5 \times 10^{19}\,\mathrm{cm}^{-2}$.

categorization, as this happened outside of our time frame and so we have no information on their asymmetries prior to the interaction. Galaxy 199 was also excluded, since its companion was failed to be removed and so it contributes to the A_{mod} calculation (see Section 2.3.3 and 4). For cases where the entire interaction only concerns one snapshot, we opted to include the snapshot immediately following it in the interaction time frame. We also decided to only consider the snapshots up to and including the final snapshot for cases where the interaction continues beyond the final snapshot, as we have no information on the target's asymmetry after the final snapshot. The distribution of our sample of interacting galaxies among these three categories is shown in Figure 11. We find a striking result: almost all galaxies that were considered for this categorization show a >10% higher mean asymmetry during the interaction compared to when they were isolated. These percentage increases ranged from ∼11% to as high as ∼74%. We also note that galaxy 287, which is the only galaxy classified as stable, already had a notably high mean asymmetry prior to the interaction, such that the interaction did not make it considerably more asymmetric. In some cases, the interaction does not seem to have many long-lasting effects after the event, but further study on the post-interaction time frame would be required to draw any firm conclusions. We also did not find significant correlations between the baryonic mass ratio of the two galaxies and how much the target's mean A_{mod} increased. However, the variety in the interactions in terms of duration, distance of the companion, etc. complicates matters, and so we are careful with drawing a conclusion from this specifically. Nonetheless, the results of our interacting sample, albeit limited in size, indicate that interactions are very likely to be directly responsible for increases in asymmetry of HI morphology. This increase in asymmetry could also point to significant amounts of HI gas being stripped from the galaxy, as that would result in especially disturbed gas distributions, which could for example affect the galaxy's star formation. Particularly dense local environments then, in which galaxies could be reasonably expected to have multiple interactions during their lifetimes, might shape the evolution of the galaxies inside them.

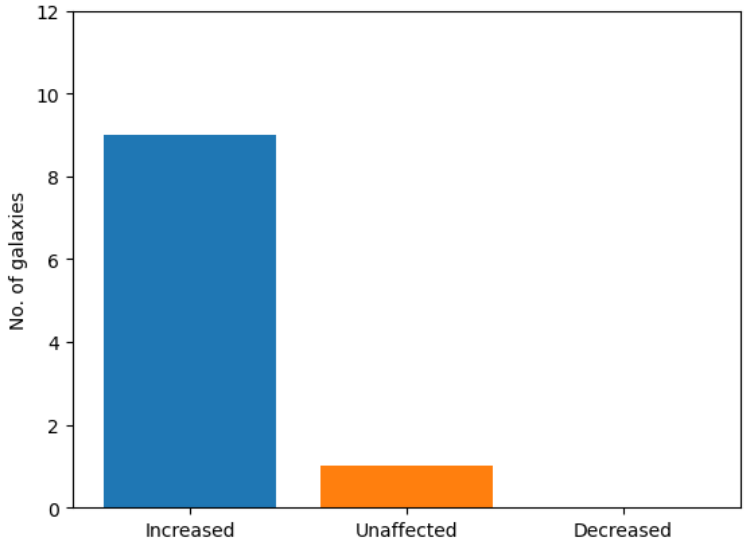

Figure 11: A distribution of how the A_{mod} of our interacting galaxies is affected by the interaction. Galaxies are categorized as increased, unaffected, or decreased based on their mean A_{mod} during the interaction compared to before the start of the interaction.

Furthermore, some plots in Figure 9 suggest that the asymmetry peaks near the pericenter. To investigate this further, we identified local maxima by simple comparison of A_{mod} values to their neighboring values, and fitted a second degree polynomials to these maxima and their surrounding points. We then calculated the vertex of these fitted polynomials as an estimate of when the asymmetry is at its highest. We only considered galaxies for which the pericenter is before snapshot 149. Figure 12 shows a comparison of the pericenter snapshot and the "location" of the peak of the fitted polynomial for these galaxies. We see that for most galaxies, the asymmetry peaks slightly after the pericenter snapshots. Physically, this could be explained by the fact that the influence of a galaxy's gravitational potential on the other galaxy gets stronger as the galaxies get closer to each other. This means that the pericenter is a point at which this influence is the strongest, while also likely being the point at which the companion moves on from the target galaxy. One could then imagine the companion galaxy "grabbing" the HI gas of the target galaxy and pulling it along as it moves away.

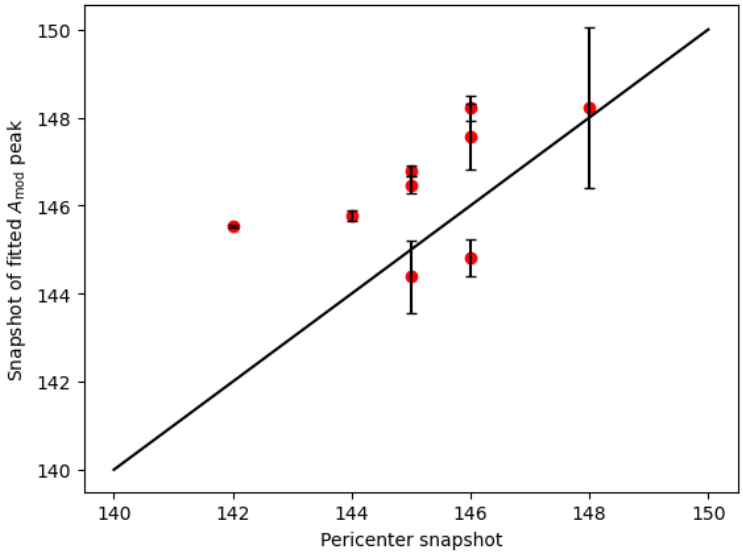

Figure 12: A comparison of the time at which we find the peak of the polynomial fitted to A_{mod} and the pericenter snapshots. The solid black line shows the line of equality, where the time of the peak and the pericenter coincide. The errorbars display the uncertainty of the fitted peak.

3.3 Mergers

As explained in Section 2.3.1, our merger sample consists of 12 galaxies that have experienced an increase of >5% in both their baryonic and stellar mass due to merging with a companion galaxy. Figure 13 shows A_{mod} plotted against the snapshot number for our 12 merger galaxies. There seem to be several instances of a galaxy decreasing in asymmetry after the "merger moment": the moment of maximum fractional baryonic mass increase.

We categorized the merger sample further based on their A_{mod} behavior after merging. We use the same definitions for these categories as with the isolated galaxies, but instead only consider the snapshots after their "merger moment". We put galaxy 12483 in the decreasing category, despite of it not satisfying the slope criterion for it. However, it shows such a substantial drop in asymmetry that we believe it is justified to count it as decreasing. We also opted to exclude galaxy 401 from this categorization, as its merger happened only at the very end of our

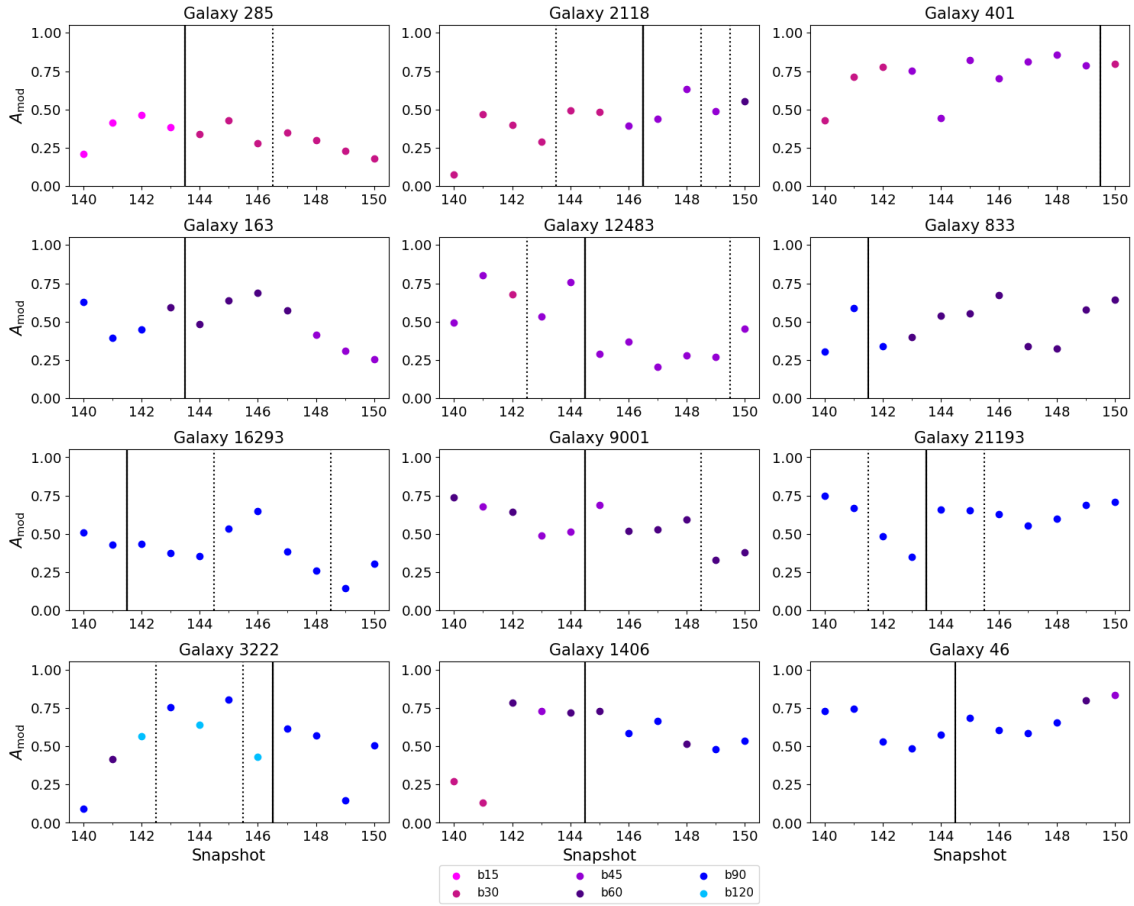

Figure 13: A mosaic of the evolution of A_{mod} across the considered snapshot range for our merger galaxies. The points in each plot are again colored to indicate the beam size used in that snapshot. The black lines (both dotted and solid) indicate the snapshots in between which a simultaneous >5% increase was detected in a galaxy's stellar and baryonic mass. The solid black line represents where the fractional increase in baryonic mass was the highest. Galaxies in the same row are in the same mass bin.

considered snapshots such that the "post-merger" time frame could not be properly analyzed. Figure 14 shows how the galaxies are distributed across these categories. We find that ∼64% of the merger galaxies that were considered for further categorization decrease in asymmetry after their maximum baryonic mass increase. We also find no meaningful relation between the behavioral category a galaxy was placed in and its exact value of fractional baryonic mass increase, nor its baryonic mass. However, we do find that the slopes of the asymmetry trends might depend on the time frame over which a galaxy experiences its baryonic and stellar mass increases, how often it has these mass acquisitions. Galaxies that had more points of baryonic and stellar mass increase spread out over a longer time frame tended to decrease less steeply in asymmetry than galaxies with less points of mass increase over a shorter time frame, especially if these multiple fractional mass increases were similar to each other in size. If we take the slopes to be an indication of the time scale needed for galaxies to settle their HI discs, and the time over which substantial increases happen as an indication of the time scale of the merging process, then this could suggest that the time needed for reorganization of the HI disc primarily depends on the duration of the merging process. However, we were unable to fully quantify this correlation, and it might be weak to moderate at best. Further study would be required to draw any firm conclusions. It does not seem physically unreasonable for this to be the case however, since a longer merging process will have more time to disrupt the HI disc.

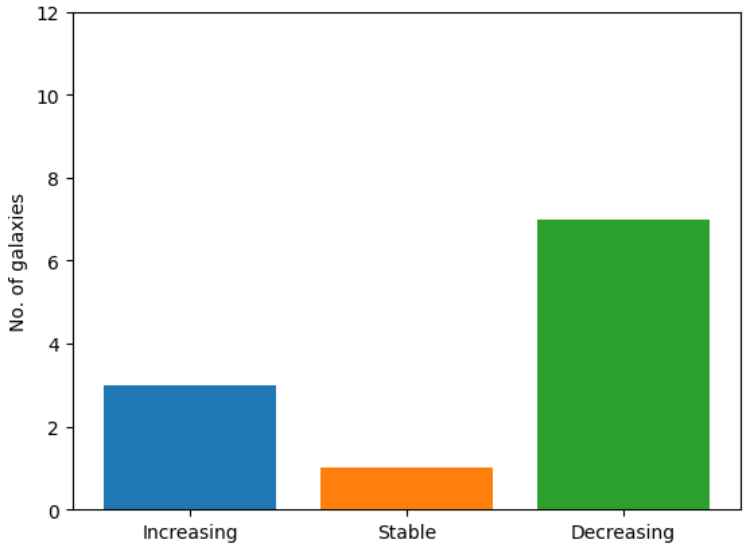

Figure 14: A distribution of the general A_{mod} behavior in our merger sample after the maximum fractional increase of baryonic mass. Galaxies are categorized as increasing, stable, or decreasing in A_{mod}.

3.4 Comparison of the centers

We now investigate the prospect of using the kinematic center and the HI morphological center as proxies for the potential minimum, as they are easily accessible centers in real observations. While we suspect the kinematic center to be a suitable proxy in particular, we still wish to investigate the difference between the two. The method for determining both centers is laid out in 2.4.

Figure 15 shows a side by side comparison of the positions of both the kinematic and morphological center relative to that of the potential minimum. The top row in the figure shows where

the centers would be located in a moment-0 map, with the black cross indicating the location of the potential minimum. The bottom row shows a distribution of the distance between the potential minimum and each respective center. We see from Figure 15 that the kinematic center gives a much better estimate of the location of the potential minimum than the morphological center, given that there is a large peak near 0 and only a small trail of higher values in its distance histogram. This result is not necessarily surprising, as the kinematic center should tell us approximately around which point the disc is rotating, which will also generally be the potential minimum.

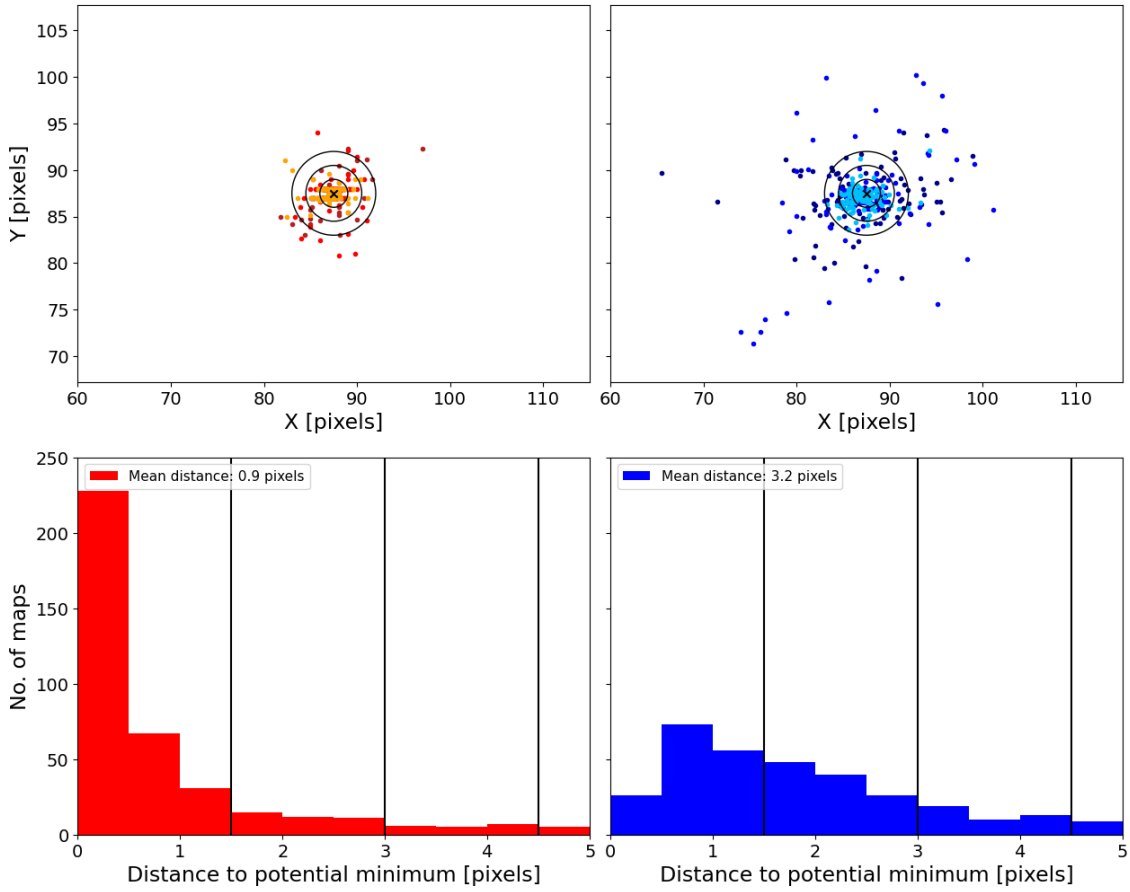

Figure 15: A comparison of the positions of the kinematic (*left*) and HI morphological (*right*) centers for all moment-0 maps relative to the potential minimum. The top row displays the actual positions of the centers in the moment-0 coordinate axes. The black cross indicates the location of the potential minimum, and the black circles represent the sizes of the 15", 30" and 45" beams. The bottom row shows a histogram of how the distance between the centers and the potential minimum is distributed among all moment-0 maps. The black lines indicate the radii of the 15", 30" and 45" beams. The colors of the data points in the top row represent if it corresponds to a merger (*dark red/dark blue*), an interacting galaxy (*red/blue*) or an isolated galaxy (*orange/light blue*).

To compare how the A_{mod} measurement is influenced by our choice of different centers, we plot this "re-centered" A_{mod} against its original values acquired from rotation around the potential minimum. The plots for both respective centers are shown in Figure 16. The dotted lines indicate a difference of ± 0.15 with respect to the original A_{mod} value. The value of 0.15 is

motivated by our categorization of low, medium and high $A_{\rm mod}$ at the end of Section 2.3.1. For example, a galaxy with $A_{\rm mod} = 0.45$, an average medium $A_{\rm mod}$, would instead be classified as having high or low $A_{\rm mod}$ if it differed by more than 0.15. When we rotate around our calculated kinematic center, ∼80% of the data points are still within this $A_{\rm mod} \pm 0.15$ range compared to ∼49% for the morphological center. About half (∼40% in total) of those data points for the kinematic center differed by less than 0.005 from the original $A_{\rm mod}$, being almost equal.

From Figure 16, we also find that we are much more likely to underestimate a galaxy's asymmetry if the morphological center is used, especially at higher asymmetries. Since the morphological center is calculated as a "center of mass", a particularly strong asymmetric feature can significantly influence the result by shifting the center towards it, thereby minimizing the asymmetry. If we use the kinematic center, we find that we overestimate the asymmetry in some cases. Since some galaxies are more complex than the one illustrated in Figure 5, it is possible that the mean value of the pixels in the moment-1 map is not an accurate assumption of the systemic velocity in more complicated systems, especially not when the companion and target are intertwined and not adequately separated (see Section 2.3.3). This can lead to an incorrect estimate for the systemic velocity contour and us consequently misidentifying high dispersion regions as possible kinematic center candidates. We find several of these cases in our moment maps, where there seems to be a promising high dispersion region near the potential minimum that is not considered to be a possible kinematic center, because it is simply too far from the estimated systemic velocity contour. We suspect that a more refined and sophisticated approach to finding the kinematic center is likely to resolve this issue. Therefore, for real observations, we suggest the use of the kinematic center to emulate the potential minimum, as the morphological HI center is likely to provide misleading results for the asymmetry.

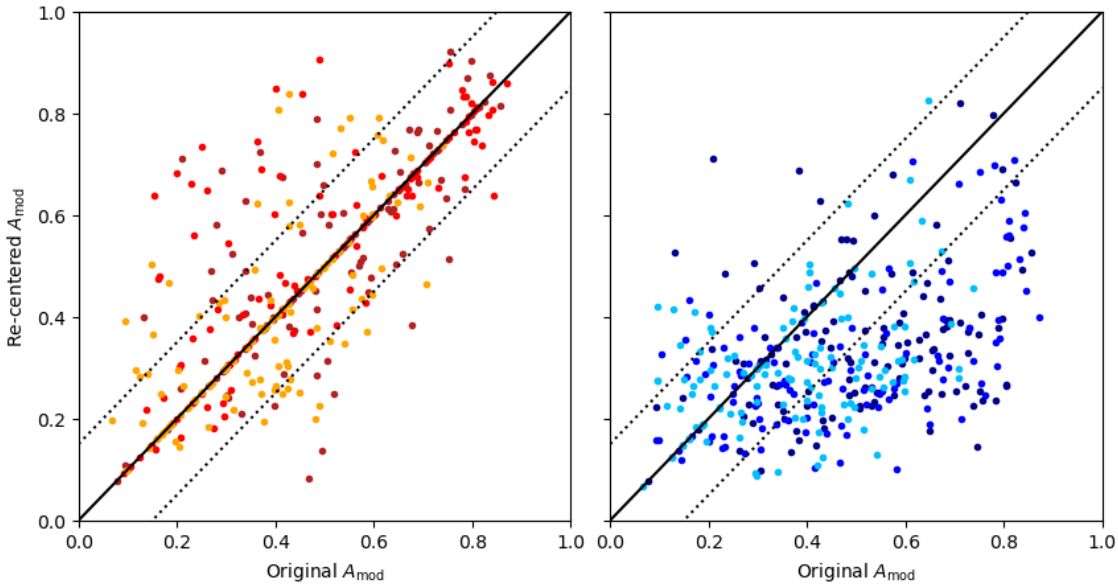

Figure 16: $A_{\rm mod}$ when the center of rotation is taken to be the kinematic center (*left*) and the morphological center (*right*). The solid black line represents the line of equality with the original $A_{\rm mod}$. The dotted black lines enclose a range of ±0.15 with respect to the line of equality. The colors represent if the data point corresponded to a merger (*dark red/dark blue*), an interacting galaxy (*red/blue*) or an isolated galaxy (*orange/light blue*).

4 Discussion

This chapter will provide a discussion of some issues that presented themselves during this work. Section 4.1 discusses some individual galaxies that displayed some notable behavior during further analysis. Section 4.2 will briefly describe some limitations we encountered, most of which have already been mentioned as they came up.

4.1 Peculiarities in the categories

4.1.1 Isolated galaxies

Galaxy 7162, the isolated galaxy with the steepest increase in its asymmetry, seems to actually be undergoing an interaction. As was briefly touched on in Section 2.3.1, it is likely that its companion did not satisfy the >5% baryonic mass criterion for it to be classified as an interacting galaxy. Figure 17 shows four unmasked moment-0 maps for galaxy 7162, with an approaching companion and interaction clearly visible. Below that are the corresponding masked/smoothed moment-0 maps, on which we did the A_{mod} calculation. The effect of the interaction is still very apparent, especially because the cube masking did not seem to adequately remove the companion. Galaxy 9, the galaxy with the second steepest increase, appears to owe its increasing asymmetry to its HI disc shifting around the potential minimum. The galaxy displays no notable asymmetries otherwise and a look at its stellar and HI mass shows that it is dominated by stellar mass (∼88% of its baryonic mass), so we think it is plausible that the galaxy's heavy stellar component and its HI disc are slightly offset from each other. Figure 18 displays three masked/smoothed moment-0 maps that we performed the A_{mod} calculation on for galaxy 9, showing how its HI disc slightly moves around the potential minimum. This could mean the galaxy is slightly lopsided, but the HI disc itself seems to stay mostly symmetric, so we consider this trend to caused by Martini's specific choice of coordinate system. Since the two aforementioned galaxies owe their increasing asymmetries to our own misclassification of an interacting galaxy and the coordinate system of the cubes respectively, we attribute their trends to data processing. We also wish to note that galaxy 5337, despite being classified as stable overall, shows a peaking asymmetry in the first half of the time frame. The moment-0 maps did not show any "trigger" for this peak, but the galaxy did display some signatures that suggested a previous interaction. We therefore believe it is perhaps still recovering from an interaction that happened prior to our considered time frame. The aforementioned galaxies appear to be the main culprits for the isolated galaxies having similarly high A_{mod} variance as the other two categories, which was briefly touched on at the start of Chapter 3. We also suspect that some of the shifting that occurred for galaxy 9 happens with other galaxies as well, leading to fluctuations in asymmetry despite not showing these variations physically. This is further elaborated on in Section 4.2.

4.1.2 Mergers

Two out of three galaxies in the "increasing" category for the mergers displayed some unique behavior. In the case of galaxy 2118 for example, the increasing A_{mod} is paired with a continuously increasing baryonic mass, suggesting it might still be actively merging. However, its moment-0 maps suggest that the cores already fully merge after snapshot 143 (see Figure 19). This is also supported by the fact that there is a big jump of ∼58% in its stellar mass at that moment, with a baryonic mass increase of ∼16% as well. The other points of >5% baryonic mass increase seem to be attributable to an increasing HI mass, with relatively small increases in stellar mass still (∼7-9%, enough to classify it as a merger). The baryonic mass for this galaxy is also dominated by HI, making it particularly sensitive to increases in HI mass. The moment-0 maps show that

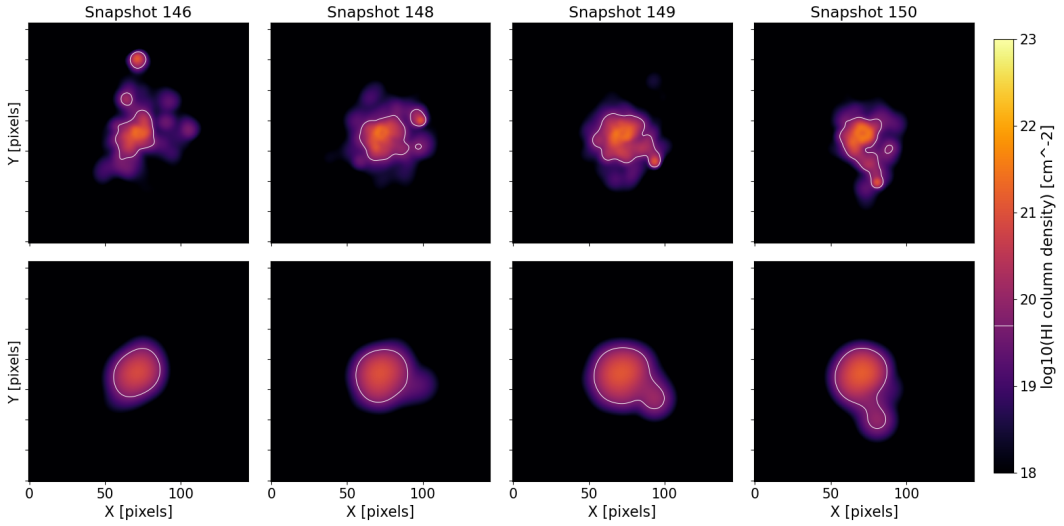

Figure 17: Some unmasked (*top*) and masked/smoothed (*bottom*) moment-0 maps of galaxy 7162, showing the approach and effects of a companion galaxy. The white contour shows where the HI column density is $5 \times 10^{19}\,\mathrm{cm}^{-2}$.

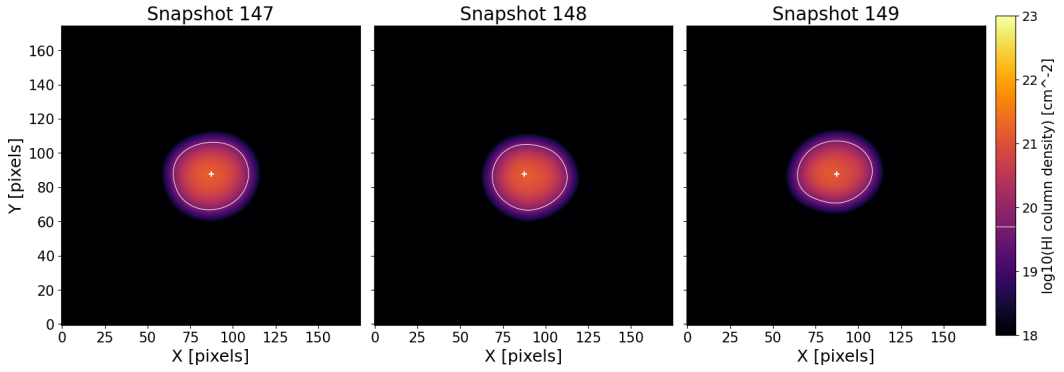

Figure 18: Some masked and smoothed moment-0 maps of galaxy 9, showing how the galaxy moves around the potential minimum. The potential minimum, corresponding to the center of the images, is indicated by the white cross. The white contour shows where the HI column density is $5 \times 10^{19}\,\mathrm{cm}^{-2}$.

the companion comes at our target with a very large tail, which is still present after the cores merge. We suspect that over time, more parts of this tail are gradually counted as belonging to our target galaxy, which would be reflected by a continuous increase in HI/baryonic mass and asymmetry. Galaxy 46 on the other hand, experiences a substantial loss of ∼70% in HI mass over the last 3-4 snapshots. This is also where its asymmetry starts to increase the most. Examining its instantaneous star formation rate at the different snapshots reveals that this decrease in HI mass is paired with an increase in its star formation rate (see Figure 20), suggesting that the HI gas is being used for star formation. The increase in stellar mass corresponded to approximately a third of the decrease in HI mass, though this is not visible in Figure 20 due to the stellar mass component being much larger. Another possibility is that some HI is ionized due to feedback mechanisms, which means it is not included in the mock data cube anymore and therefore not visible in the moment-0 maps.

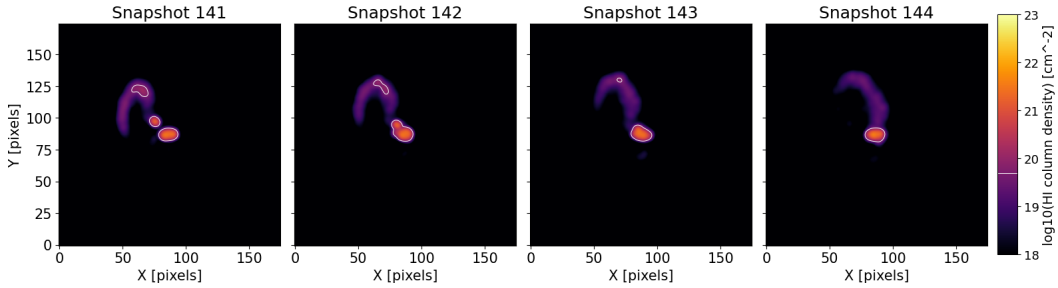

Figure 19: Some unmasked moment-0 maps of galaxy 2118, showing the merging of the cores. The white contour shows where the HI column density is $5 \times 10^{19}\,\mathrm{cm}^{-2}$.

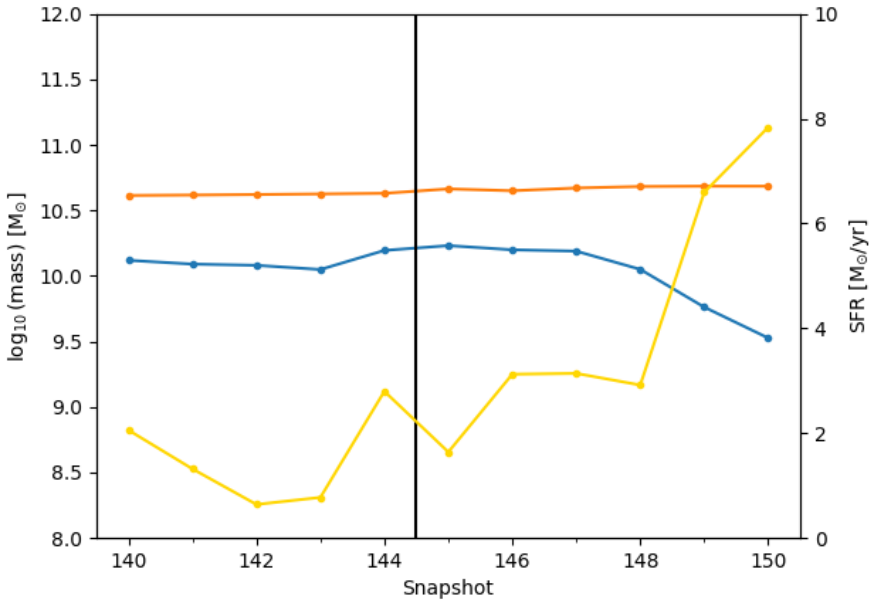

Figure 20: Evolution of HI mass (*blue*), stellar mass (*orange*) and instantaneous star formation rate (*yellow*) for galaxy 46. The lines connecting the data points are solely for the purpose of clarity. The solid black line again indicates the moment of maximum baryonic mass increase.

4.2 Limitations

Section 2.3.3 briefly mentioned that our method of masking was sometimes inadequate in removing the companions when the two galaxies were particularly connected. This happened primarily for the merger galaxies, which we did not find problematic to consider as one system. However, two interacting galaxies still had their companion not be removed by our masking. These galaxies were therefore not considered for further analysis. A more accurate source detection and method of assigning HI to the correct source in such cases is of course preferred, but was not feasible within the scope of this work.

Our categorization of the galaxies only considered the presence of a companion within our studied range of snapshot to classify galaxies as isolated, interacting or merging. However, this leaves the possibility for isolated galaxies to have experienced a merger or interaction just prior to the start of our considered time frame, from which it could still be recovering. Furthermore, some interactions spanned the entirety of our time frame and some mergers only happened at the end, which meant we could not properly analyze their effects. Ideally, we would have briefly examined a few snapshots before and after our time frame to rule out such cases, which would improve our analysis of the samples.

As touched on in Section 3.4, our determination for the kinematic center was likely not sophisticated enough for it to reliably distinguish what appeared to be the true kinematic center, especially for complicated systems. We suspect this is due to looking for high dispersion regions along the systemic velocity contour, which we took to be the mean velocities of the pixels in the moment-1 map. However, it is possible that this does not correspond to the true systemic velocity in some cases, leading to an incorrect estimate. We also found that our method sometimes picked out other high dispersion regions that did not correspond to the kinematic center in particularly "chaotic" systems. However, we do still suspect that the kinematic center is an excellent proxy for the potential minimum if one is able to reliably find it. Careful examination of the data cubes, the moment-1 maps and the moment-2 maps may be required to provide an accurate estimate for more complex systems.

We found that galaxies sometimes appeared to shift slightly with respect to the image center, leading to fluctuations or increases in their asymmetry despite being fairly symmetric in morphology otherwise. This is likely an effect of Martini's choice of coordinate system, which sets the image center to be the potential minimum, which could be slightly offset from the center of the HI discs. While these fluctuations were mostly drowned out by actual physical increases in asymmetry for the interacting systems and mergers, the isolated galaxies sometimes suffered relatively high variations in asymmetry because of this. We tried to combat this by using a robust regression line method that was not sensitive to such outliers.

5 Summary and Conclusions

In this study, we investigated the evolution of morphological asymmetry in the HI discs of 36 simulated galaxies, equally distributed across three categories: isolated, interacting, and merging galaxies. These galaxies were selected from the SIMBA simulations, a suite of cosmological simulations of galaxy formation. For 11 snapshots in time spanning the last ∼2.3 Gyr, we produced moment-0 maps of our simulated galaxies and used those to calculate the asymmetry of their HI discs at each snapshot. This allowed us to investigate how the morphological HI asymmetry changes over time, and how this is related to the environmental processes represented by each category. A brief description of the three categories and our key findings are laid out below.

For the isolated galaxies, we analyzed the evolution of their asymmetries over the entire ∼2.3 Gyr time frame and categorized them further based on trends in this evolution. Galaxies were categorized as increasing, stable or decreasing based on these trends. Our findings showed that ∼67% of the galaxies in our sample were either stable (50%), or slightly decreasing (∼17%) in asymmetry. This suggests that the HI discs of isolated galaxies are not likely to show noteworthy trends in the asymmetry of their HI distribution.

For our sample of 12 interacting galaxies, we studied how the interaction as a whole affected the target galaxy, which is considered to be isolated before the approach of the companion galaxy. For 10 of these galaxies, we were able to compare the mean asymmetry before the interaction to the mean asymmetry during the interaction, further categorizing them as increased, unaffected or decreased. We found that almost all of the 10 galaxies showed an increase of >10% in their mean asymmetry during the time frame of the interaction compared to its isolated state, with only one being classified as stable. From this, we conclude that interactions are very likely to cause asymmetries in the HI distribution of a galaxy, which possibly points to the removal of significant amounts of HI gas. Additionally, we found that this asymmetry tends to be the highest shortly after the companion's closest approach. We suggest a plausible physical reason to be that the increased influence of the companion's gravitational potential at this moment allows it to pull some of the target's HI gas with it as it moves away.

For our 12 merger galaxies, we took the snapshot at which the target galaxy had experienced its highest increase in baryonic mass as a proxy for the moment it merged with its companion galaxy. We then categorized our sample further as increasing, stable, or decreasing based on general trends in the asymmetry of our galaxies after this "merger moment". We found that ∼64% of the categorized mergers show a decreasing trend in their asymmetries after merging. The steepness of this trend appeared to be correlated with the number of mass increases and how they were spread out, but not the target galaxy's baryonic mass or its relative increase. This would imply that the time needed for the HI disc to settle primarily depends on the duration of the merging process, which will continuously disrupt the HI disc for a longer period of time. However, further study would be required to draw firm conclusions on this matter.

The three categories were chosen to roughly represent the different way in which a galaxy could interact with its environment, mainly with other neighboring galaxies. Our findings from these three samples then grant useful insight into how these kinds of processes can affect the HI distribution of galaxies. While it is difficult to really grasp the effects on a galaxy's further evolution from changes in morphology alone, asymmetries in the HI disc are also thought to be correlated to processes related to gas accretion or removal. We have shown that interactions and mergers actively contribute to these disruptions in HI morphology, which means that the resulting asymmetries in morphology can be used to understand the dynamical processes that take place between galaxy pairs. Characterizing such processes further could then improve our understanding of what may have affected a galaxy's evolution in the past, possibly allowing us

to trace it back to what kind of environment it resided in previously.

In addition to investigating the evolution of morphological HI asymmetries, we looked into the prospect of using more easily accessible centers as a proxy for the potential minimum, given that the latter is not something one has access to in real observations. The centers we considered were the kinematic center and the HI morphological center. We found that one tends to underestimate the asymmetry if the HI morphological center is used, as it is very susceptible to the influence of asymmetric features on its calculation. For the kinematic center, our results showed that it did not differ significantly from the position of the potential minimum in the majority of cases, and that it provided similar enough values of asymmetry for $\sim$80% of the moment-maps. We suspect that a more refined approach to its calculation will yield even more successful results. We therefore suggest the kinematic center as a suitable stand-in for the potential minimum in real observations, should one study the morphological HI asymmetry in a similar manner as done in this thesis.

Our galaxies were selected from a larger sample that is the subject of a future study (N. Hank, in preparation). The morphological, kinematic and spectral asymmetries of the galaxies in this parent sample will be studied in more detail. Their mock HI observations are constructed to resemble observations of a population of galaxies in the Abell 262 cluster from the Medium-Deep HI imaging survey (MDS), and will be compared to these real observations.

Acknowledgements

We acknowledge the use of the ilifu cloud computing facility - www.ilifu.ac.za, a partnership between the University of Cape Town, the University of the Western Cape, Stellenbosch University, Sol Plaatje University, the Cape Peninsula University of Technology and the South African Radio Astronomy Observatory. The ilifu facility is supported by contributions from the Inter-University Institute for Data Intensive Astronomy (IDIA - a partnership between the University of Cape Town, the University of Pretoria and the University of the Western Cape), the Computational Biology division at UCT and the Data Intensive Research Initiative of South Africa (DIRISA).

A special thanks to Marc, Nadine, and Filippo for their supervision throughout this project, I am really grateful for all of their guidance. Another special thanks goes to Sarah for her involvement and enthusiasm for the project, and the many useful discussions. Finally, a heartfelt thank you to my friends for all the shared struggles and fun times throughout not just this thesis period, but the entire bachelor's. You gave me the motivation I needed in some of the hard times during the degree (and there were many).

References

Adams, E. and van Leeuwen, J. (2019). Radio surveys now both deep and wide. *Nature Astronomy*, 3:188.

Angiras, R. A., Jog, C. J., Omar, A., and Dwarakanath, K. S. (2006). Origin of disc lopsidedness in the Eridanus group of galaxies. *Monthly Notices of the Royal Astronomical Society*, 369(4):1849–1857.

Anglés-Alcázar, D., Davé, R., Faucher-Giguère, C.-A., Özel, F., and Hopkins, P. F. (2017). Gravitational torque-driven black hole growth and feedback in cosmological simulations. *MNRAS*, 464(3):2840–2853.

Baldwin, J. E., Lynden-Bell, D., and Sancisi, R. (1980). Lopsided galaxies. *MNRAS*, 193:313–319.

Bilimogga, P. V., Oman, K. A., Verheijen, M. A. W., and van der Hulst, T. (2022). Using eagle simulations to study the effect of observational constraints on the determination of Hi asymmetries in galaxies. *Monthly Notices of the Royal Astronomical Society*, 513(4):5310–5327.

Bondi, H. (1952). On Spherically Symmetrical Accretion. *Monthly Notices of the Royal Astronomical Society*, 112(2):195–204.

Bournaud, F., Combes, F., Jog, C. J., and Puerari, I. (2005). Lopsided spiral galaxies: evidence for gas accretion. *AA*, 438(2):507–520.

Choque-Challapa, N., Aguerri, J. A. L., Mancera Piña, P. E., Peletier, R., Venhola, A., and Verheijen, M. (2021). The dwarf galaxy population in nearby clusters from the KIWICS survey. *Monthly Notices of the Royal Astronomical Society*, 507(4):6045–6060.

Chynoweth, K. M., Langston, G. I., Yun, M. S., Lockman, F. J., Rubin, K. H. R., and Scoles, S. A. (2008). Neutral hydrogen clouds in the m81/m82 group. *The Astronomical Journal*, 135(6):1983.

Cramer, W. J., Kenney, J. D. P., Sun, M., Crowl, H., Yagi, M., Jáchym, P., Roediger, E., and Waldron, W. (2019). Spectacular hubble space telescope observations of the coma galaxy d100 and star formation in its ram pressure–stripped tail. *The Astrophysical Journal*, 870(2):63.

Davé, R., Anglés-Alcázar, D., Narayanan, D., Li, Q., Rafieferantsoa, M. H., and Appleby, S. (2019). simba: Cosmological simulations with black hole growth and feedback. *Monthly Notices of the Royal Astronomical Society*, 486(2):2827–2849.

Davé, R., Thompson, R., and Hopkins, P. F. (2016). mufasa: galaxy formation simulations with meshless hydrodynamics. *Monthly Notices of the Royal Astronomical Society*, 462(3):3265–3284.

de Blok, W. J. G., Walter, F., Ferguson, A. M. N., Bernard, E. J., Hulst, J. M. v. d., Neeleman, M., Leroy, A. K., Ott, J., Zschaechner, L. K., Zwaan, M. A., Yun, M. S., Langston, G., and Keating, K. M. (2018). A high-resolution mosaic of the neutral hydrogen in the m81 triplet. *The Astrophysical Journal*, 865(1):26.

Deb, T., Verheijen, M. A. W., and van der Hulst, J. M. (2023). An H I story of galaxies in Abell 2626 and beyond. , 676:A118.

Duc, P.-A. and Bournaud, F. (2008). Tidal Debris from High-Velocity Collisions as Fake Dark Galaxies: A Numerical Model of VIRGOHI 21. *ApJ*, 673(2):787–797.

Gunn, J. E. and Gott, J. Richard, I. (1972). On the Infall of Matter Into Clusters of Galaxies and Some Effects on Their Evolution. *ApJ*, 176:1.

Hibbard, J. E., van Gorkom, J. H., Rupen, M. P., and Schiminovich, D. (2001). An hi rogues gallery.

Hopkins, P. F. (2015). A new class of accurate, mesh-free hydrodynamic simulation methods. *Monthly Notices of the Royal Astronomical Society*, 450(1):53–110.

Hopkins, P. F. and Quataert, E. (2011). An analytic model of angular momentum transport by gravitational torques: from galaxies to massive black holes. *Monthly Notices of the Royal Astronomical Society*, 415(2):1027–1050.

Hotan, A. W. et al. (2021). *Publications of the Astronomical Society of Australia*, 38:e009.

Hubble, E. P. (1926). Extragalactic nebulae. *ApJ*, 64:321–369.

Huber, P. J. (1964). Robust Estimation of a Location Parameter. *The Annals of Mathematical Statistics*, 35(1):73 – 101.

Jarvis, M. et al. (2016). In *MeerKAT Science: On the Pathway to the SKA*, page 6.

Johnston, S. et al. (2008). *Experimental Astronomy*, 22:151.

Kennicutt, Robert C., J. (1998). Star Formation in Galaxies Along the Hubble Sequence. , 36:189–232.

Koribalski, B. S. et al. (2020). *Astrophysics and Space Science*, 365:118.

Krumholz, M. R., McKee, C. F., and Tumlinson, J. (2009). The Atomic-to-Molecular Transition in Galaxies. II: H I and H_2 Column Densities. *ApJ*, 693(1):216–235.

Lelli, F., Verheijen, M., and Fraternali, F. (2014). The triggering of starbursts in low-mass galaxies. *Monthly Notices of the Royal Astronomical Society*, 445(2):1694–1712.

Maddox, N. et al. (2021). *Astronomy Astrophysics*, 646:A35.

Manuwal, A., Ludlow, A. D., Stevens, A. R. H., Wright, R. J., and Robotham, A. S. G. (2021). Drivers of asymmetry in synthetic Hi emission-line profiles of galaxies in the eagle simulation. *Monthly Notices of the Royal Astronomical Society*, 510(3):3408–3429.

Mapelli, M., Moore, B., and Bland-Hawthorn, J. (2008). Lopsided galaxies: the case of NGC 891. *Monthly Notices of the Royal Astronomical Society*, 388(2):697–708.

Meyer, M., Robotham, A., Obreschkow, D., Westmeier, T., Duffy, A. R., and Staveley-Smith, L. (2017). Tracing HI Beyond the Local Universe. , 34:52.

Nelson, D., Pillepich, A., Springel, V., Weinberger, R., Hernquist, L., Pakmor, R., Genel, S., Torrey, P., Vogelsberger, M., Kauffmann, G., Marinacci, F., and Naiman, J. (2017). First results from the IllustrisTNG simulations: the galaxy colour bimodality. *Monthly Notices of the Royal Astronomical Society*, 475(1):624–647.

Oman, K. A. (2019). MARTINI: Mock spatially resolved spectral line observations of simulated galaxies. Astrophysics Source Code Library, record ascl:1911.005.

Oman, K. A. (2024). Martini: Mock array radio telescope interferometry of the neutral ism. *Journal of Open Source Software*, 9(98):6860.

Oman, K. A., Marasco, A., Navarro, J. F., Frenk, C. S., Schaye, J., and Benítez-Llambay, A. (2018). Non-circular motions and the diversity of dwarf galaxy rotation curves. *Monthly Notices of the Royal Astronomical Society*, 482(1):821–847.

Planck Collaboration XIII (2016). Planck 2015 results - xiii. cosmological parameters. *AA*, 594:A13.

Rahmati, A., Pawlik, A. H., Raičević, M., and Schaye, J. (2013). On the evolution of the H I column density distribution in cosmological simulations. *MNRAS*, 430(3):2427–2445.

Reynolds, T. N., Westmeier, T., Staveley-Smith, L., Chauhan, G., and Lagos, C. D. P. (2020). Hi asymmetries in LVHIS, VIVA, and HALOGAS galaxies. *Monthly Notices of the Royal Astronomical Society*, 493(4):5089–5106.

Sancisi, R., Fraternali, F., Oosterloo, T., and van der Hulst, T. (2008). Cold gas accretion in galaxies. , 15(3):189–223.

Schade, D., Lilly, S. J., Crampton, D., Hammer, F., Fèvre, O. L., and Tresse, L. (1995). Canada-france redshift survey: Hubble space telescope imaging of high-redshift field galaxies*. *The Astrophysical Journal*, 451(1):L1.

Schaye, J., Crain, R. A., Bower, R. G., Furlong, M., Schaller, M., Theuns, T., Dalla Vecchia, C., Frenk, C. S., McCarthy, I. G., Helly, J. C., Jenkins, A., Rosas-Guevara, Y. M., White, S. D. M., Baes, M., Booth, C. M., Camps, P., Navarro, J. F., Qu, Y., Rahmati, A., Sawala, T., Thomas, P. A., and Trayford, J. (2014). The eagle project: simulating the evolution and assembly of galaxies and their environments. *Monthly Notices of the Royal Astronomical Society*, 446(1):521–554.

Schmidt, M. (1959). The Rate of Star Formation. *ApJ*, 129:243.

Smith, B. D., Bryan, G. L., Glover, S. C. O., Goldbaum, N. J., Turk, M. J., Regan, J., Wise, J. H., Schive, H.-Y., Abel, T., Emerick, A., O'Shea, B. W., Anninos, P., Hummels, C. B., and Khochfar, S. (2017). GRACKLE: a chemistry and cooling library for astrophysics. *MNRAS*, 466(2):2217–2234.

Turk, M. J., Smith, B. D., Oishi, J. S., Skory, S., Skillman, S. W., Abel, T., and Norman, M. L. (2010). yt: A multi-code analysis toolkit for astrophysical simulation data. *The Astrophysical Journal Supplement Series*, 192(1):9.

van Cappellen, W. A. et al. (2022). *Astronomy Astrophysics*, 658:A146.

Verheijen, M., Oosterloo, T., Heald, G., and van Cappellen, W. (2009). Panoramic radio astronomy: Wide-field 1-2 ghz research on galaxy evolution. In *Proceedings of the Panoramic Radio Astronomy Conference*, page 10.

Verheijen, M. A. W., Oosterloo, T. A., van Cappellen, W. A., Bakker, L., Ivashina, M. V., and van der Hulst, J. M. (2008). The evolution of galaxies through the neutral hydrogen window. In Minchin, R. and Momjian, E., editors, *American Institute of Physics Conference Series*, volume 1035, pages 265–271.

Vogelaar, M. G. R. and Terlouw, J. P. (2001). Astronomical data analysis software and systems x. In Harnden, F. R. J., Primini, F. A., and Payne, H. E., editors, *Astronomical Society of the Pacific Conference Series*, volume 238, page 358.

Watts, A. B., Power, C., Catinella, B., Cortese, L., and Stevens, A. R. H. (2020). Global Hi asymmetries in IllustrisTNG: a diversity of physical processes disturb the cold gas in galaxies. *Monthly Notices of the Royal Astronomical Society*, 499(4):5205–5219.

Zaritsky, D. and Rix, H.-W. (1997). Lopsided spiral galaxies and a limit on the galaxy accretion rate*. *The Astrophysical Journal*, 477(1):118.